ARTICLE

Zinc on the edge—isotopic and geophysical evidence that cratonic edges control world-class shale-hosted zinc-lead deposits

David L. Huston[1] · David C. Champion[1] · Karol Czarnota[1] · Jingming Duan[1] · Matthew Hutchens[1,2] ·
Suzanne Paradis[3] · Mark Hoggard[4] · Bryant Ware[5] · George M. Gibson[4] · Michael P. Doublier[1] · Karen Kelley[6] ·
Anne McCafferty[6] · Nathan Hayward[3] · Fred Richards[7] · Svetlana Tessalina[5] · Graham Carr[8]

Abstract

The North Australian Zinc Belt is the largest zinc-lead province in the world, containing three of the ten largest known individual deposits (HYC, Hilton-George Fisher, and Mount Isa). The Northern Cordillera in North America is the second largest zinc-lead province, containing a further two of the world's top ten deposits (Red Dog and Howards Pass). Despite this world-class endowment, exploration in both mineral provinces during the past 2 decades has not been particularly successful, yielding only two significant discoveries (Teena, Australia, and Boundary, Canada). One of the most important aspects of exploration is to choose mineral provinces and districts within geological belts that have the greatest potential for discovery. Here, we present results from these two zinc belts that highlight previously unused datasets for area selection and targeting. Lead isotope mapping using analyses of mineralized material has identified gradients in μ ($^{238}U/^{204}Pb$) that coincide closely with many major deposits. Locations of these deposits also coincide with a gradient in the depth of the lithosphere-asthenosphere boundary determined from calibrated surface wave tomography models converted to temperature. Furthermore, gradients in upward-continued gravity anomalies and a step in Moho depth correspond to a pre-existing major crustal boundary in both zinc belts. A spatial association of deposits with a linear mid- to lower-crustal resistivity anomaly from magnetotelluric data is also observed in the North Australian Zinc Belt. The change from thicker to thinner lithosphere is interpreted to localize prospective basins for zinc-lead mineralization and to control the gradient in lead isotope and geophysical data. These data, when combined with data indicative of paleoenvironment and changes in plate motion at the time of mineralization, provide new exploration criteria that can be used to identify prospective mineralized basins and define the most favorable parts of these basins.

Keywords Shale-hosted zinc deposits · Cratonic edges · Lead isotopes · Lithospheric-asthenospheric boundary · Upward-continued gravity · Magnetotellurics

Introduction

Sediment-dominated basins are by far the largest global source of zinc and lead, containing 54% and 68%, respectively, of the world's endowment of these metals (Huston et al. 2022). The giant size of some of these deposits makes them attractive exploration targets. However, they are difficult to find as they are rarer than other zinc-lead deposits such as volcanic-hosted massive sulfide (VHMS) deposits. Despite their attractiveness, very few major sediment-hosted zinc-lead deposits have been discovered in the past 2 decades. One possible reason has been a poor understanding of fundamental, large-scale controls on mineralization. Given that hundreds of sedimentary basins exist in the world, the following are key questions addressed in this study: (1) are there ways to screen more prospective from less prospective basins, and (2) are there ways to determine the most prospective parts of favorable basins?

The North Australian Zinc Belt, which is hosted by the Paleo- to Mesoproterozoic North Australian Basin System (Southgate et al. 2000, 2013), is the richest zinc province in the world, containing a total endowment of 89 Mt Zn and

41 Mt Pb—10% and 13%, respectively, of global pre-mining resources of these metals (Huston et al. 2022). The Northern Cordillera of western North America (Siberling et al. 1992; Colpron et al. 2006; Nelson et al. 2013), which extends from the northwestern conterminous USA through western Canada and into Alaska, is another major zinc province, containing a total endowment of 72 Mt Zn and 33 Mt Pb (Huston et al. 2022). A striking feature of both zinc-lead provinces is that each had several distinct mineralizing events that occurred over a period of many tens to hundreds of millions of years. In both provinces metallogenic lightning has struck twice, actually many times, raising the possibility that some fundamental feature of these metallogenic provinces has enhanced the metal endowment.

In this contribution, we build on previous work by Hobbs et al. (2000), Southgate et al. (2013), Gibson et al. (2017), Hoggard et al. (2020), Huston et al. (2020), and Hayward and Paradis (2021). Hobbs et al. (2000) presented evidence that the major zinc-lead deposits of the North Australian Zinc Belt are associated with a prominent gravity "worm," which marks a horizontal gradient in upward-continued gravity data. Southgate et al. (2013) and Gibson et al. (2017) also presented evidence that zinc-lead deposits in this belt and parts of the Northern Cordillera are associated with the edges of continental shelves or platforms. Here, we present evidence that the distribution of basin-hosted zinc-lead deposits in these provinces is fundamentally controlled by cratonic edges that are visible in multiple datasets, including lead isotope, potential field, surface-wave tomographic, reflection seismic, and magnetotelluric data. Although lead isotope, reflection seismic, and magnetotelluric data are restricted in coverage due to acquisition logistics, potential field data (e.g., gravity and magnetic) are available globally, albeit at different resolutions, in addition to a range of global tomographic models (c.f. Hoggard et al. 2020). The continuity of these latter datasets over large parts of the world facilitates their first-order use to identify prospective basins at the global, continental, and province scales (Lawley et al. 2022).

All of the above datasets are used herein to answer the two key questions identified above. We demonstrate that basin-hosted zinc-lead deposits are associated with cratonic edges and that the resolutions of different datasets enable their use at different stages of exploration. Moreover, as the datasets presented in this study reflect different geochemical and geophysical properties of the host provinces, using all in combination provides new and more robust insights into geological processes that control basin-hosted zinc-lead deposits and districts. Although we have concentrated on zinc, it is possible or even likely that some of the same datasets can be used in understanding the genesis of, and exploration for, other types of basin-hosted mineral deposits, as demonstrated by Hoggard et al. (2020) for sediment-hosted copper deposits.

Basin-hosted zinc-lead deposits—timing of mineralization and terminology

Sedimentary basins host a wide range of zinc-lead deposits, some clearly epigenetic, but others formed either during sedimentation or early diagenesis. Although Mississippi Valley–type deposits are generally accepted products of as epigenetic mineralization that formed after lithification of the host rocks (Leach et al. 2005; Wilkinson 2014), the timing of shale-hosted[1] zinc-lead mineralization has been the topic of significant debate during the last half-century. Some authors (Williams 1978; Kelley et al. 2004a,b; Gadd et al. 2016, 2017; Johnson et al. 2015, 2018; Slack et al. 2017; Spinks et al. 2021) have advocated an early diagenetic timing, whereas others have argued for deposition during sedimentation (Carne and Cathro 1982; Goodfellow et al. 1993; Large et al. 2005) or during late diagenesis or basin inversion (Broadbent et al. 1998; Gibson et al. 2017). Advocates of the syn-sedimentary timing have termed these shale-hosted deposits "SEDEX" (sedimentary exhalative: Carne and Cathro 1982), historically the most commonly used term for these deposits. Given the significant debate as to the timing of mineralization, we prefer to use a purely descriptive term such as "shale-hosted" rather than SEDEX. Leach et al. (2005) proposed the term "clastic-dominated" (CD) as an alternative non-genetic term.

At about the same time that the term SEDEX was coined, Morganti (1981) proposed a classification of basin-hosted, stratiform deposits by basin type, recognizing three types: (1) intracratonic basin–type deposits, (2) flysch basin–type deposits, and (3) platformal-marginal–type deposits. We have used the philosophy of assessing basin environment for deposit classification and adapted the Morganti (1981) approach along the lines used by Barrie and Hannington (1999) for VHMS deposits. In this classification of VHMS deposits, classifications are based on the lithological succession that hosts the deposit. For shale-hosted zinc-lead deposits, we recognize two types, siliciclastic-mafic and siliciclastic-carbonate (see also Hofstra et al. 2021). The former includes deposits hosted by siliciclastic-dominated basins with significant syn-depositional mafic igneous rocks (basaltic lavas and volcaniclastic rocks or high-level mafic sills) but without volumetrically major carbonate units. The siliciclastic-carbonate type, in contrast, refers to deposits hosted by basins with abundant siliciclastic and carbonate units but that mostly lack coeval mafic igneous rocks. The siliciclastic-mafic type corresponds to the flysch basin type of Morganti (1991), whereas the siliciclastic-carbonate

---

[1] Although in many cases, the host rocks include siltstone we use the term "shale" to refer to any very-fine-grained siliciclastic sedimentary rock.

type corresponds to the intracratonic basin and platformal-marginal types.

Our classification is also broadly consistent with the classification of Cooke et al. (2000), which is also based indirectly on the characteristics of basin fill. Cooke et al. (2000) inferred that their McArthur-type deposits were formed from oxidized brines produced by oxidized basins, whereas their Selwyn-type deposits were formed from reduced brines produced by reduced basins. The McArthur-type deposits correspond broadly to our siliciclastic-carbonate type, and the Selwyn type corresponds broadly to our siliciclastic-mafic types.

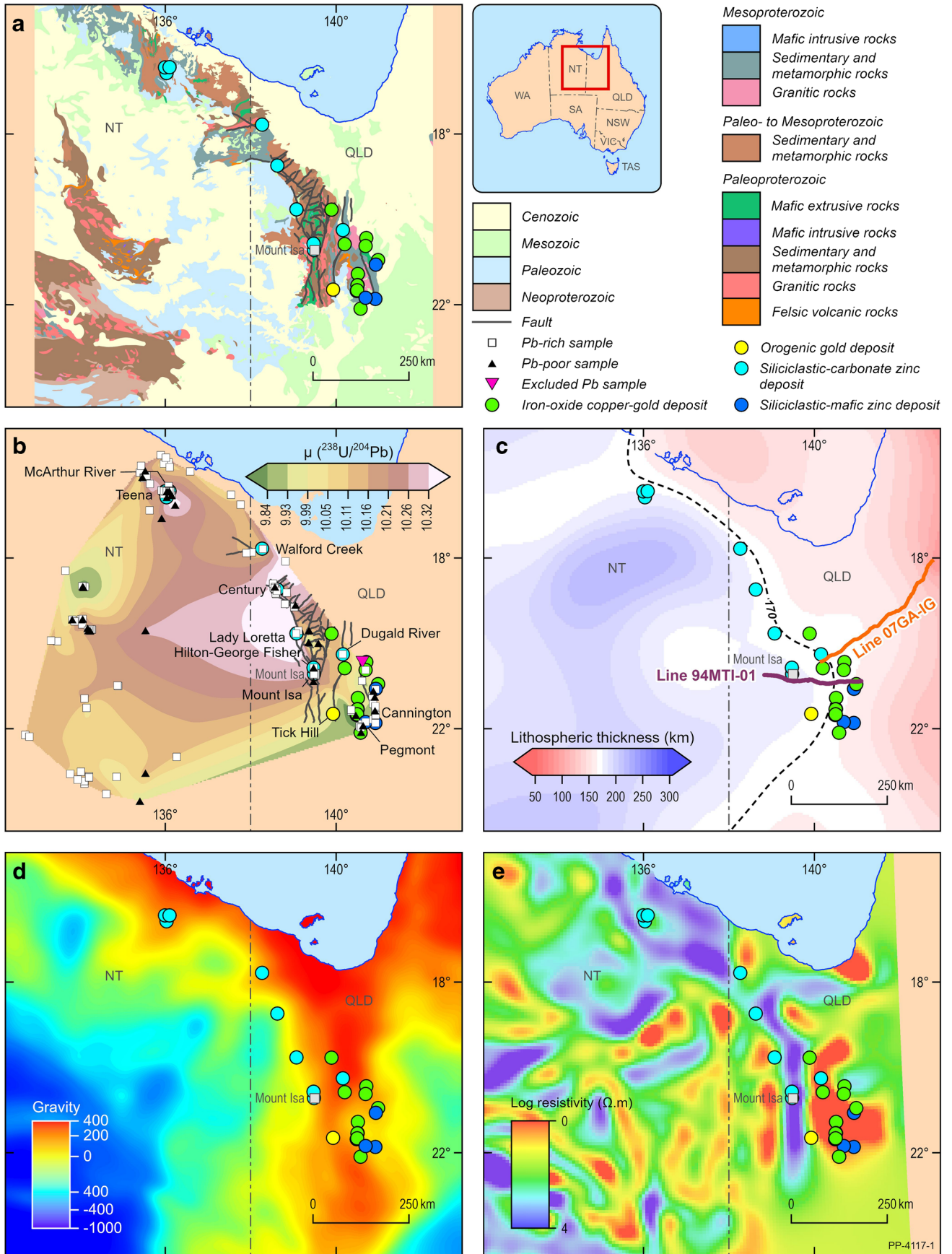## The North Australian Zinc Belt

The North Australian Zinc Belt (Fig. 1) contains three of the ten largest zinc-lead deposits in the world (McArthur River [HYC—Here's-Your-Chance], Hilton-George Fisher, and Mount Isa), as well as several smaller, yet still important, deposits (Century, Dugald River, Teena, Lady Loretta, and Cannington). Among these, only Teena is a recent (2013) discovery (Taylor et al. 2017). In addition, significant copper-cobalt and zinc-lead resources are being defined at the Walford Creek deposit (Valenta 2020).

Figure 1a shows the surface geology of the North Australian Zinc Belt and the location of sediment-hosted zinc-lead, sediment-hosted copper-cobalt, iron oxide-copper–gold, and orogenic gold deposits. The North Australian Basin System, which hosts the North Australian Zinc Belt, has been subdivided into three superbasins: the 1790–1740 Ma Leichhardt, the 1730–1640 Ma Calvert, and the 1640–1595 Ma Isa superbasins (Southgate et al. 2013; Gibson et al. 2016). The Leichhardt Superbasin consists of a rift, filled with continental tholeiites, fluvial to lacustrine siliciclastic rocks, and minor carbonate rocks (Jackson et al. 2000; Gibson et al. 2018). Figure 2 shows a schematic east–west cross-section illustrating sedimentary facies assemblages and spatial and temporal relationships of the Calvert Superbasin and the locations of basin-hosted deposits within the various facies assemblages. The Calvert Superbasin consists of shallow-marine siliciclastic and carbonate rocks in the west, with deeper-marine siliciclastic rocks in the east, that mostly lack carbonates but contain coeval mafic sills and possible lavas (Fig. 2; Jackson et al. 2000; Southgate et al. 2013; Withnall and Hutton 2013; Gibson et al. 2018). Deposition of the siliciclastic-dominated succession in the east coincided with erosion and development of the Gun unconformity and emplacement of granitic rocks to the west (Neumann et al. 2009). With the conclusion of rifting and rift-related magmatism toward the end of Calvert time, passive margin conditions became widely established across northern Australia. The uppermost Isa Superbasin postdates passive

margin formation and consists of fluviatile to deep-marine sandstone, siltstone, and dolostone (Southgate et al. 2000).

The North Australian Basin System has been compartmentalized into third- and fourth-order sub-basins by long-lived, north-northeast- and northwest-striking faults (Fig. 1a). The former are steep to subvertical and thought to have been inherited from the underlying ≥ 1840 Ma crystalline basement (Gibson et al. 2017; Hejrani et al. 2020). The northwest-striking faults were mainly developed during formation of the Calvert Superbasin as a right-stepping *en echelon* array of crustal-scale normal faults along the western margin of the Lawn Hill and Mount Isa regions, where the majority of zinc deposits are located (Fig. 1a). This fault array originated during northeast–southwest-directed extension and broadly marks the western limits of bimodal magmatism and lithospheric thinning that took place during and before formation of the Calvert Superbasin (possibly indicating a craton edge). Together with the older basement faults, these Calvert-age faults were reactivated during later basin-forming events and strongly influenced the location and distribution of younger, more easterly trending sub-basins of the Isa Superbasin. Calvert-age faulting and rift-related basaltic magmatism concluded at or before ca. 1655 Ma, to be followed by thermal subsidence, basin inversion, and orogenesis from ca. 1650 to ca. 1640 Ma (Riversleigh Event; Withnall and Hutton 2013; Gibson et al. 2017). Subsequent to the Riversleigh Event, extension resumed in a north–south-directed orientation and continued until ca. 1620 Ma when terminated by the onset of the Isan Orogeny (e.g. Gibson et al. 2017). Orogenesis and sedimentation in the Isa Superbasin ended around 1575 Ma. No basaltic rocks are present in this basin with the exception of minor, but locally abundant, tuff units (e.g., Davidson and Dashlooty 1993) and late ca. 1620 Ma rhyolite sills; the basin was largely amagmatic (Gibson et al. 2018).

The shale-hosted zinc-lead deposits are hosted by slope facies of the Calvert and Isa superbasins (Figs. 1a and 2). The oldest deposits, which include the siliciclastic-mafic Cannington and Pegmont deposits, formed at ca. 1680 Ma in the eastern, siliciclastic-dominated, mafic-rich part of the Calvert Superbasin. Siliciclastic-carbonate deposits are hosted by the platform/shelf facies of the Calvert and the Isa superbasins, including the ca. 1665 Ma Dugald River deposit, the ca. 1655 Ma Mt Isa and Hilton-George Fisher deposits, the ca. 1645 Ma Lady Loretta, the ca. 1640 Ma McArthur River and Teena deposits, and the ca. 1575 Ma Walford Creek and Century deposits. All of these deposits are hosted by dolomitic and carbonaceous siltstone units within successions that contain abundant carbonate but lack significant volcanic rocks. Southgate et al. (2013) and Gibson et al. (2017) indicated that these deposits are associated with the transition between shallow-water shelf and deeper-water basinal environments. These settings bring together

a

Mesoproterozoic
- Mafic intrusive rocks
- Sedimentary and metamorphic rocks
- Granitic rocks

Paleo- to Mesoproterozoic
- Sedimentary and metamorphic rocks

Paleoproterozoic
- Mafic extrusive rocks
- Mafic intrusive rocks
- Sedimentary and metamorphic rocks
- Granitic rocks
- Felsic volcanic rocks

- Cenozoic
- Mesozoic
- Paleozoic
- Neoproterozoic
- Fault
- □ Pb-rich sample
- ▲ Pb-poor sample
- ▼ Excluded Pb sample
- ● Iron-oxide copper-gold deposit
- ● Orogenic gold deposit
- ● Siliciclastic-carbonate zinc deposit
- ● Siliciclastic-mafic zinc deposit

0   250 km

b

$\mu\ (^{238}U/^{204}Pb)$

9.84 9.93 9.99 10.05 10.11 10.16 10.21 10.26 10.32

McArthur River
Teena
Walford Creek
Century
Lady Loretta
Hilton-George Fisher
Mount Isa
Tick Hill
Dugald River
Cannington
Pegmont

c

Line 07GA-IG
Line 94MTI-01
170
Mount Isa

Lithospheric thickness (km)

50 100 150 200 250 300

0   250 km

d

Gravity

400
200
0
400
400
1000

Mount Isa

0   250 km

e

Log resistivity (Ω.m)

0

4

Mount Isa

0   250 km

PP-4117-1

◄**Fig. 1** Maps of North Australian Zinc Belt showing **a** simplified surface geology (Raymond et al 2012), **b** variations in *μ* as determined from lead isotope analyses from mineral deposits and occurrences (Carr et al 2001; this study: Appendix E1; indicated faults are from Murphy et al 2011), **c** variations in depth of lithosphere-asthenosphere boundary as determined from surface-wave tomography (Hoggard et al. 2020), **d** 30-km upward-continued Bouguer anomaly map (Lane et al. 2020), and **e** conductivity model at a depth of 36 km using data from the AusLAMP magnetotelluric survey (Duan et al. 2021). Locations of significant mineral deposits are overlain as different symbol types. Traces of reflection seismic lines 94MTI-01 and 07GA-IG1 are shown in part (**c**)

the essential mineral system components of saline basinal brines, source rocks, and the deposition of mixed reductants and carbonates necessary for the deposition of zinc and lead sulfide minerals (Large et al. 2005).

The Northern Cordillera of western North America

The northern segment of the Cordilleran Orogen of western North America (Northern Cordillera) has a large and diverse metallogenic endowment that reflects its diverse geology and a protracted tectonic history that occurred along and offshore of the western and northern Laurentian continental margin since Mesoproterozoic time (Fig. 3a). The Red Dog (Alaska) and Howards Pass (Yukon-Northwest Territories) siliciclastic-carbonate and Sullivan (British Columbia) siliciclastic-mafic-deposits are among the largest shale-hosted, zinc-lead deposits in the world (Leach et al. 2005). Smaller deposits of similar type in proximity to these include the Anarraaq, Lik, and Aktigiruq deposits in the Red Dog district; the Drenchwater deposit in the central Brooks Range (all siliciclastic-carbonate deposits); the Tom, Jason, and recently discovered Boundary deposits in the Macmillan Pass district (Yukon); and the Faro, Dy, Grum, Swim, and Vangorda deposits in the Anvil district (Yukon). Barite deposits are spatially and/or genetically related to many of these Zn-Pb deposits (Moore et al. 1986; Goodfellow et al. 1993; Fernandes et al. 2017; Magnall et al. 2020), and in the Brooks Range of Alaska, some of the barite bodies are extraordinarily large (~ 1 Gt: Kelley et al. 2004a; Kelley and Jennings 2004; Johnson et al. 2004). Sub-seafloor replacement of carbonate (e.g., Kelley et al. 2004a) or barite (Kelley et al. 2004b; Magnall et al. 2020) by metal-bearing fluids has been documented as an important factor for sulfide deposition in many of these deposits. Gibson et al. (2017) indicated that in the Selwyn Basin, like the North Australian Zinc Belt, many of the deposits are spatially associated with the transition from shallower-water shelf into deeper-water basinal environments.

The Northern Cordillera includes autochthonous and parautochthonous strata of the western North American

margin and allochthonous, mobile crustal fragments (terranes) that formerly resided in the northeastern Pacific Ocean basin. The tectonic collage was built up through the amalgamation of terranes and their accretion to the continental margin between late Paleozoic and Cenozoic time (Nelson et al. 2013). The geologic terranes have diverse origins and histories and are generally grouped by cratonic associations, lithotectonic setting, and tectonic evolution (e.g., Coney et al. 1980; Silberling et al. 1992; Colpron et al. 2006).

The eastern part of the Northern Cordillera consists of autochthonous and parautochthonous continental margin rocks deposited along the western margin of Laurentia, or the North American Craton, together with overlying Proterozoic to Triassic cover rocks. The North American Craton extends beneath part of the Cordillera (Ross 1991; Cook et al. 2012; Nelson et al. 2013; Hayward 2015). During the early Paleozoic, shallow-water platformal strata and adjacent deeper water basinal strata were deposited along the margin.

In the southern part of the Northern Cordillera, the North American Craton is dominated by the Belt-Purcell Basin. This a Mesoproterozoic, clastic-dominated basin that contains the giant Zn-Pb-Ag Sullivan deposit as well as the Ag-Pb–Zn Coeur d'Alene Cordilleran vein district in Idaho. At ca. 1475 ± 4 Ma (Slack et al. 2020) and ca. 1500 Ma (Ramos and Rosenberg 2012), respectively, these are the oldest zinc-lead deposits that formed along the western margin of the North American Craton.

West of the craton and continental margin rocks, the Northern Cordillera consists of allochthonous terranes, most of which accreted to the margin beginning in the Permian and continuing into Cretaceous time. These terranes include volcanic, plutonic, sedimentary, and metamorphic assemblages of the peri-Laurentian, Arctic-northeastern Pacific, and Coastal "realms" that originated as magmatic arcs, accretionary complexes, microcontinents, and floors of ocean basins (Nelson et al. 2013). The Intermontane terranes of the peri-Laurentian "realm" (Yukon-Tanana, Quesnel, Stikine) have affinities to western Laurentia (North American Craton) and evolved west of the margin following establishment of outboard subduction zones in the Devonian. The Intermontane terranes were progressively accreted to the margin from Permian closure of the Slide Mountain marginal ocean to terminal amalgamation in the Jurassic (Murphy et al. 2006).

Terranes of Arctic-northeastern Pacific affinity lie west and north of the peri-Laurentian terranes. The Arctic terrane is a large, composite allochthonous crustal block that originated in the northeastern Arctic region near Baltica (Miller et al. 2011) or from Laurentia (Canadian Arctic or Atlantic margin: Strauss et al. 2013). These rocks constitute Neoproterozoic to Paleozoic continental shelf-slope strata and younger peri-cratonic rocks of the southern Brooks Range
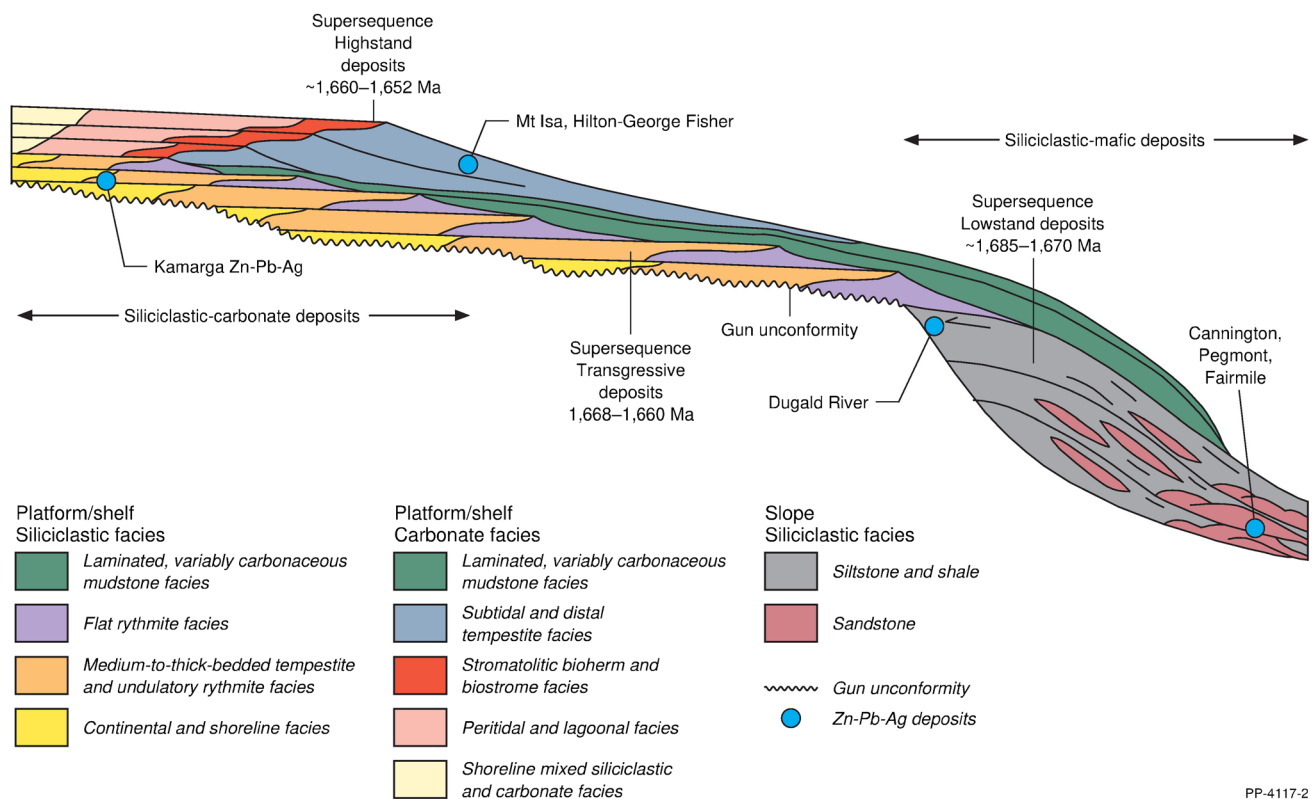
Fig. 2 Schematic east–west cross-section illustrating facies assemblages and spatial and temporal relationships of the Leichhardt and Calvert Superbasins in the North Australian Zinc Belt. Schematic locations of shale-hosted deposits are shown to illustrate relationships with superbasin architecture and evolution. Modified after Southgate et al. (2013)

(Moore et al. 1994). The continental fragments that make up the Arctic terrane were derived from both Laurentia and Baltica, which were juxtaposed against northern Laurentia during the Devonian to Mississippian (Strauss et al. 2013) and then underwent collisional orogenesis in the Brooks Range during the Mesozoic (Till 2016). The Arctic terrane also includes the Seward Peninsula, which is primarily underlain by metamorphosed Neoproterozoic to middle Paleozoic rocks with Baltica affinity (Till et al. 2014).

The rest of Alaska, south of the Brooks Range and outboard of the Laurentian and peri-Laurentian terranes, is made up of a diverse assemblage of pericratonic, arc, and oceanic terranes (Western Alaska in Fig. 3a) that were predominately accreted during the Mesozoic (e.g., Ridgway et al. 2002; Trop and Ridgway 2007; Hampton et al. 2010; Box et al. 2019).

Post-Caledonian (Devonian-Mississippian) extension, which affected both Arctic Alaska and the western margin of the North America Craton (Miller et al. 2011), provided the setting for formation of some of the major sediment-hosted sulfide and barite deposits. The westward drift of the North American Craton during Cretaceous and early Paleogene time caused intense compressional deformation in the Cordillera and focused in two plutonic-metamorphic

belts (Monger and Gibson 2019), the Coastal plutonic complex and the Omineca Belt (not shown in Fig. 3a), which separate the three main divisions of the Cordillera: the outer Arctic-northeastern Pacific (Outboard and Insular) terranes, the central peri-Laurentian (Intermontane terranes), and the North American Craton.

In addition to the Mesoproterozoic deposits, mineralizing events occurred in the Northern Cordillera during the Paleozoic at younger than ca. 560 Ma (Cottonbelt district, British Columbia), ca. 520 Ma (Anvil Range district, Yukon Territory), ca. 440 Ma (Howards Pass district, Yukon Territory), and ca. 380–365 Ma (Macmillan Pass district, Yukon Territory, and Gataga district, British Columbia) (Paradis et al. 1998; Goodfellow 2007; Kuiper et al. 2011; Kelley et al. 2016).

Methods and data sources

Although a relationship between continental margins and the distribution of shale-hosted zinc-lead deposits has been inferred by Nelson et al. (2002) and Leach et al. (2005), identification of such margins in complexly deformed terranes is difficult. In this contribution, we show that a range
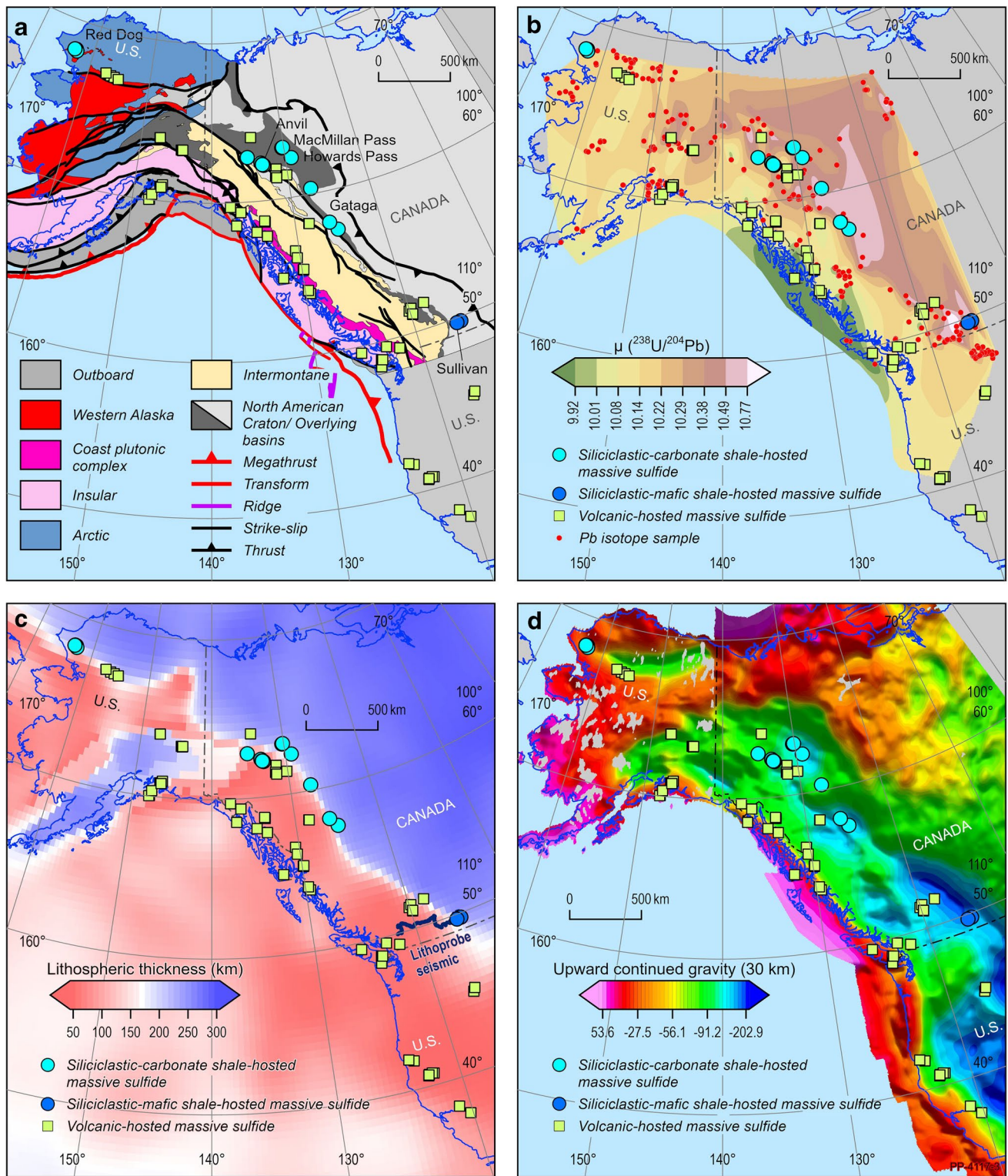
Fig. 3 Maps of the Northern Cordillera of western North America showing **a** simplified surface geology (Colpron and Nelson 2020), **b** variations in μ as determined from lead isotope analyses from mineral deposits and occurrences (Church et al. 1987; Thorpe 2008: Appendix E2), **c** variations in the depth of lithosphere-asthenosphere boundary as determined from surface wave tomography (Hoggard et al. 2020), and **d** 30-km upward-continued Bouguer anomaly map (Phillips et al. 1993; Saltus et al. 2008; Geological Survey of Canada 2017). The locations of significant mineral deposits are overlain as different symbols. The trace of Southern Canadian Cordillera reflection seismic traverse is shown in part (**c**)

of geochemical and geophysical datasets can be used to map these margins and can, when combined with basin characteristics, identify prospective provinces at global to district scales.

Lead isotope data

The distribution of lead isotope data is irregular as these were collected almost exclusively from mineral deposits and occurrences. The North Australian Zinc Belt and the Northern Cordillera have among the spatially densest lead isotope coverages in the world. For the North Australian Zinc Belt, we have used the dataset of Carr et al. (2001) supplemented by new data collected as part of this study (Appendix E1). For the Northern Cordillera, our combined dataset is mostly from Church et al. (1987) and Thorpe (2008) (Appendix E2).

All lead isotope analyses were obtained from galena and other ore minerals such as pyrite or from gossans. Analyses were divided into two groups, lead-rich (samples with Pb ≥ 1000 ppm) and lead-poor (< 1000 ppm Pb). For lead-rich samples, measured ratios were inferred to approximate initial ratios. For lead-poor samples, initial ratios were calculated by removing ingrown lead where lead, uranium, and thorium concentration data were available and an estimate of the age of mineralization could be made. The initial ratios were used to calculate isotopic ratios using the lead isotope evolution model of Stacey and Kramers (1975).

As many of the deposits/occurrences have yielded multiple analyses, the most precise and least radiogenic (with oldest model age) analysis was used for data contouring. In addition, to guard against extreme ingrowth, which can significantly affect μ, the dataset was culled to remove analyses with young model ages, which can result in anomalously high μ. This process took into account varying ages of deposits and is summarized in Appendix E3. In general, lead-poor samples with model ages 100 Myr younger than the deposit age range in the region were culled from the dataset. Lead-rich analyses were not culled except for samples hosted by younger basins (these samples commonly have anomalously radiogenic J-type lead). Contouring was undertaken using the Esri ArcGIS v10.8.1 average nearest-neighbor tool following the methods of Champion and Huston (2016).

Surface wave tomography

Surface waves are a form of seismic energy that travels along the interface between the ground and atmosphere. These seismic waves have typical periods of 10 to 500 s and exhibit dispersive behavior, resulting in particularly high vertical resolution (~ 25 km) of seismic velocity structure in the upper ~ 300 km of the Earth. Since the seismic velocity of silicate rocks is strongly dependent on temperature, this velocity can therefore be used to map variations in the thermal structure of the conducting lithosphere, which is related to lateral changes in plate thickness. In this study, we adopt the scheme of Richards et al. (2020), which uses a recent parameterization for anelastic deformation of mantle rocks at seismic frequencies that is calibrated using independent estimates of mantle temperature structure from oceanic plate cooling models and continental geotherms derived from xenocryst thermobarometry.

We constructed a background upper mantle seismic velocity structure using the global tomographic model SL2013sv (Schaeffer and Lebedev 2013), locally enhanced with higher resolution regional models FR12 in Australia (Fishwick and Rawlinson 2012) and SL2013NA in North America (Schaeffer and Lebedev 2014). Having converted these velocities to temperature, lithospheric thickness is estimated using the depth of the 1175 °C isotherm. Additional details, including data and maps, can be found in Hoggard et al. (2020).

Gravity data

Gravity data measure changes in the gravitational field related to the distribution of mass, including lateral changes in rock density from the Earth's surface to the core. The grids of Bouguer gravity were calculated from national databases available for Australia (Lane et al. 2020), the conterminous USA (Phillips et al. 1993), Alaska (Saltus et al. 2008), and Canada (Geological Survey of Canada 2017). For the Northern Cordillera, 2-km grids of the Bouguer gravity anomalies were merged from Canada, Alaska, and the conterminous USA to create a seamless Bouguer anomaly grid across the study area. The Bouguer gravity grids for Australia and the Northern Cordillera were then upward continued[2] to 30, 50, and 100 km to evaluate how density sources and their edges, as reflected in gravity gradients, change with progressively deeper parts of the lithosphere.

Magnetotelluric data

The magnetotelluric method utilizes variations in Earth's naturally occurring magnetic field and induced electrical fields to derive resistivity structures of the crust and upper mantle. Long-period (10–10,000 s) magnetotelluric data were acquired in northern Australian as part of the Australian Lithospheric Architecture Magnetotelluric Project

---

[2] Upward continuation is a mathematical process whereby the geophysical response of potential field data (gravity and magnetic data) is modeled further away from the source. For example, upward continuation to a height of 10 km simulates the response expected from a plane flying 10 km above the surface (where the gravity data was originally gathered). Upward continuation highlights low-frequency variations in the data, which reflect deeper features.

(AusLAMP) under the Geoscience Australia's Exploring for the Future (EFTF) program. Longer-period data are sensitive to features far from the observation site, including the upper mantle, whereas shorter-period data can be used to image closer features in the middle to upper crust. Resulting 3D resistivity models at depths of ~ 10 km to ~ 200 km give insights into the distribution of conductive rocks through the lithosphere. Further details are found in Duan et al. (2021). A similar study has not been undertaken across the Northern Cordillera, precluding consideration of this dataset for that region.

Seismic reflection data

Since 1994, Geoscience Australia, in collaboration with the Geological Survey of Queensland, acquired a series of deep seismic reflection transects in northern Queensland (Korsch et al. 2012; Korsch and Doublier 2016). Over 3500 km of data were acquired on 16 traverses. Since the early 2000s, the seismic data has been acquired using three Hemi-60 vibrators with data collected to a 20 s two-way travel time. The data were processed using the Disco/Focus seismic processing package. The processed images were interpreted by a team of geologists and geophysicists from Geoscience Australia, the Geological Survey of Queensland, and collaborators from Australian universities. Korsch et al. (2012) provide information on the surveys and final interpretations; Jones et al. (2009) reported on processing methods.

Between 1984 and 1988, Lithoprobe, Canada's multidisciplinary research program for earth sciences, in collaboration with the Geological Survey of Canada, acquired seismic reflection data along a traverse in the southern part of the Northern Cordillera (location shown in Fig. 3c), just to the north of the US border (at ~ 50°N latitude). This transect extended from the North American Craton in the east to the west coast (Cook 1995; Hammer et al. 2010) and involved 19 discrete seismic lines that were merged to form the Cordilleran transect. The data were collected using four 20,000 kg vibrators to 18 s two-way travel time. Data were processed using non-standard approaches as described by Cook et al. (1992). The data were interpreted by geophysicists and geologists from Canadian universities and the Geological Survey of Canada. Clowes (1990) and Cook et al. (1992) document data acquisition, processing, and interpretation.

Results

Variations in lead isotope data

Previous studies (Huston et al. 2014; Hollis et al. 2019) have shown that variations in parameters such as μ ($^{238}U/^{204}Pb$), as determined from lead isotope data from

mineral deposits, can reveal spatial controls and indicate fertility of mineral provinces. Figure 1b shows spatial variations in μ in the North Australian Zinc Belt. Along the eastern margin of this image, μ increases from northeast to southwest. Significantly, most siliciclastic-carbonate zinc-lead deposits and the Tick Hill orogenic gold deposits are localized along a north-northwest-trending break in μ values. Deposits occurring along the break are relatively consistently spaced about 140 km apart. Iron oxide-copper–gold and siliciclastic-mafic zinc-lead deposits are located to the east of this break and are characterized by lower μ. Other parameters determined from lead isotope data, including κ ($^{232}Th/^{238}U$) and ω ($^{232}Th/^{204}Pb$), define a similar break (not shown).

In detail, the prominent north-northwest-trending break in μ appears to be *en echelon*, broadly following the trend of the northwest-trending Calvert-age (1730–1640 Ma) structures, with individual offsets or steps controlled by the position of the underlying north-northeast basement structures (Fig. 1b). As both sets of structures are thought to have been active during formation of the Calvert and Isa superbasins and related sub-basins, it would appear that variations in μ mimic development of these sub-basins along the isotopic break. Although the break in μ appears to be controlled by basement structures, the break itself cuts across the north–south grain of the surface geology and across trends in total magnetic intensity, particularly in the east.

Figure 3b shows spatial variations in μ for the Northern Cordillera. Like the North Australian Zinc Belt, all major shale-hosted zinc-lead deposits, except those of the Red Dog district, are spatially associated with a break in μ values from higher values inboard to lower values outboard of the boundary of the North American Craton and the allochthonous terranes. Further outboard of the North American Craton, the μ continues to decrease with major VHMS districts associated with zones of lowest μ, similar to the relationship noted for Archean and Paleoproterozoic VHMS deposits elsewhere in the world (Huston et al. 2014). In detail, major shale-hosted zinc-lead districts are associated with higher-order complexities in the μ distribution patterns such as re-entrants along the ancient continental margin.

Of all the datasets considered, the spatial relationship of deposits with μ gradients is spatially the most precise, but this is only possible due to the density of data in both provinces. Very few zinc-lead provinces globally have a similar density of lead isotope data. The only province with a comparable data density is the Irish Midlands, where deposits are also associated with a gradient in μ (Hollis et al. 2019). Collectively, the distribution patterns in the North Australian Zinc Belt, the Northern Cordillera, and the Irish Midlands suggest that local zones (i.e., districts) with complex variations in μ (e.g., re-entrants) may define more prospective areas within basins. As such, lead isotope datasets may be

useful in identifying new plays at the district-scale, even in brownfield provinces.

Lithosphere-asthenosphere boundary as defined by surface wave tomography

Figure 1c shows that the locations of major deposits in the North Australian Zinc Belt coincide with the transition from thicker to thinner lithosphere, mapped using surface wave tomography (Hoggard et al. 2020). All deposits in this belt—including stratiform zinc-lead deposits hosted by carbonate-rich and siliciclastic-dominated successions and epigenetic iron oxide-copper–gold deposits—are within 100 km of the 170-km thickness contour of the lithosphere-asthenosphere boundary (LAB). Major deposits are unknown outside of this corridor, even though the North Australian Basin System extends well beyond it. Similar to the lead isotope pattern, the edge of thick lithosphere cuts across the regional geological and total magnetic intensity grains to the east and north of McArthur River (compare Fig. 1b and c with Fig. 1a), suggesting a fundamental, deep-seated control on mineralization. Figure 3c shows that there is a broad correlation of basin-hosted zinc-lead deposits in the Northern Cordillera with the 170-km LAB contour, although in detail some of these deposits are located outboard of this contour (e.g., Macmillan Pass and Howards Pass districts). Hayward and Paradis (2021) suggested that the host basin may have been displaced 100 km to the northeast relative to basement.

Analysis by Hoggard et al. (2020) of a global correlation between LAB depth and the distribution of sediment-hosted deposits showed that 85% of zinc resources and 85% of copper resources in basins are located within 200 km of the 170-km contour. The correlation with the LAB, originally identified in the North Australian Zinc Belt, thus applies globally.

Gravity data

Indications that sediment-hosted zinc-lead deposits were associated with regional-scale breaks in geophysical data were originally documented by Hobbs et al. (2000). This study reported that major zinc-lead deposits in the North Australian Zinc Belt are aligned along a composite gravity "worm" or horizontal gradient in Bouguer anomaly gravity data. Persistence of this worm through upward continuation of the data indicates a major crustal discontinuity at depth.

Figure 1d illustrates variations in the Bouguer gravity anomaly for the North Australian Zinc Belt upward-continued to 30 km. The image defines a broadly north-north-west-trending gravity high in Queensland that turns to the northwest in the Northern Territory. In Queensland, this gravity high is flanked by low-gravity anomaly zones to the west and east and is transected by several northeast-trending

discontinuities that translate the southern part of the high-gravity zone to the southwest (i.e., dextral displacement). The western margin of the high gravity anomaly zone is the Rufus Fault, the eastern margin corresponds to the Gidyea Structure (Figs. 4a,b and 5), and the main discontinuity corresponds to the Quamby-Fountain Range Fault at surface. In the far south, the gravity high is truncated by the Cork Fault, which juxtaposes the North Australian Craton with the Thomson Province of the Phanerozoic Tasman Element to the southeast. Similar, though less well-defined, patterns are present in the 15-, 50-, and 100-km upward-continued images (not shown). Using the basin architecture model of Southgate et al. (2013: Fig. 2), the gravity high is associated with the outboard, deeper-water part of the basin, whereas the gravity low is associated with the inboard, shallow water part of the basin that existed during Calvert and Isa time. The horizontal gravity gradient appears to mark the continental margin during evolution of the North Australian Basin System.

Most siliciclastic-carbonate shale-hosted zinc-lead deposits are localized along the gravity gradient that defines the western margin of this high gravity anomaly, which largely coincides with the 170-km LAB contour. The McArthur and Walford Creek districts are spatially associated with re-entrants on the western margin of the gravity high. Siliciclastic-mafic shale-hosted zinc-lead deposits (e.g., Cannington) and iron-oxide copper–gold deposits (e.g., Ernest Henry) are restricted to the eastern edge of the high gravity anomaly zone. The western margin of the high gravity anomaly and the 170-km LAB contour broadly coincide to the north of Mount Isa. In the vicinity of Mount Isa, however, the gravity gradient and 170-km LAB contour diverge (compare Fig. 1c and d). The significance of this divergence is not known and requires further analysis.

Upward continuation of gravity is often used to distinguish shallow from deeper density sources (Jacobsen 1987). Although shallow sources can be uniquely identified, longer-wavelength gravity anomalies can result from either deeply buried sources or from extensively distributed shallow sources such as basins. As shallow geological features in this area comprise Phanerozoic basins without significant volcanism (Fig. 1a), the high gravity anomaly likely reflects a deep, dense feature. In upward-continued gravity anomalies at a height z, the depth of the sources is approximately $z/2$ or deeper (Jacobsen 1987). As the gravity gradient is present in the 30- 50-, and 100-km upward continuations, the change in density structure persists from the mid-crust into the lithospheric mantle. The gravity gradient associated with the siliciclastic-carbonate shale-hosted deposits separates low-density rocks to the southwest from higher-density rocks to the northeast. The Leichhardt River Trough is positioned over these denser rocks and contains a large thickness (to 8 km) of mafic igneous rocks (Bain et al. 1992).
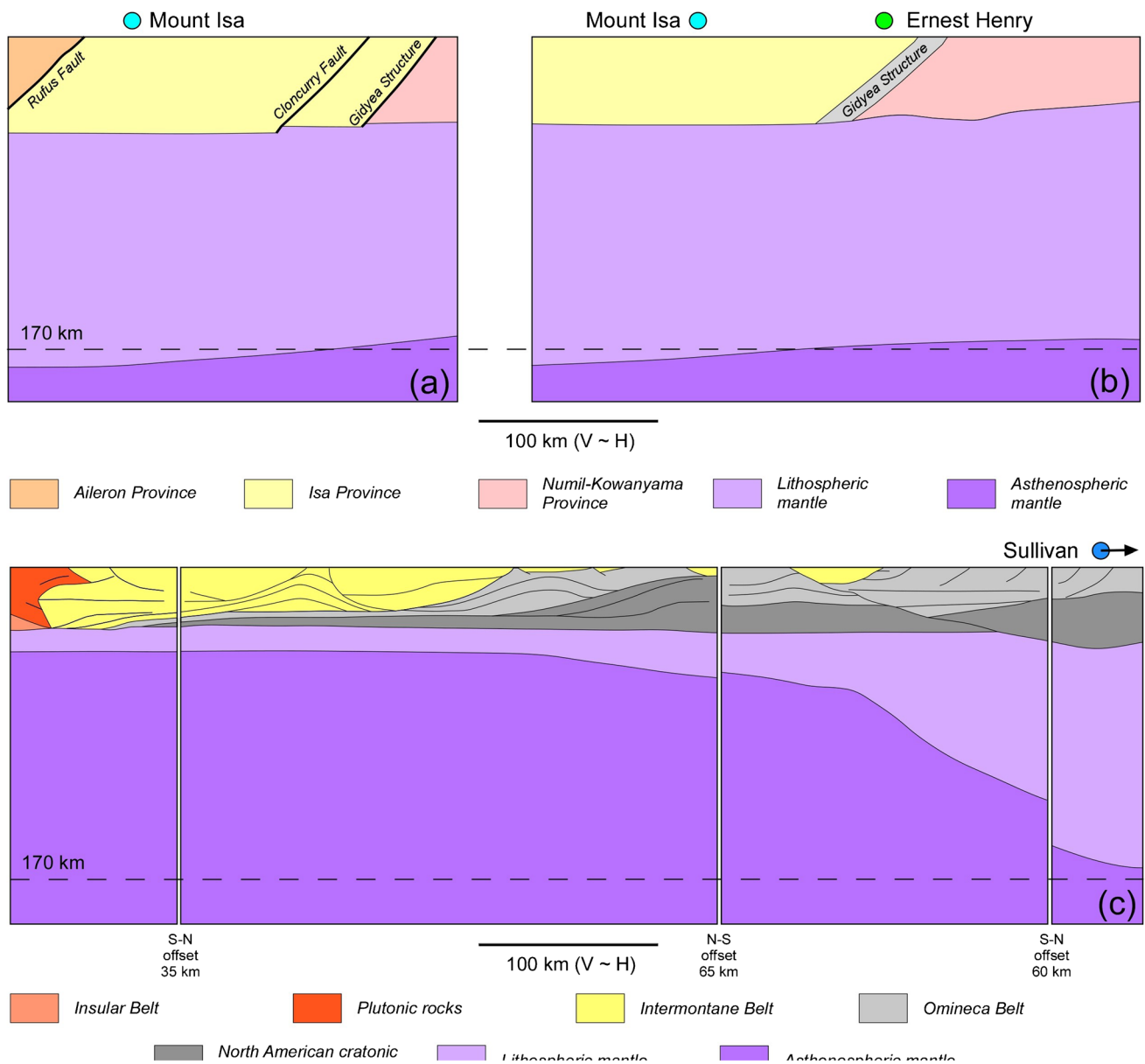
Fig. 4 Cross-sections showing architecture of the crust and lithospheric mantle based upon estimates of the depth of the lithosphere-asthenosphere boundary (Hoggard et al. 2020) and seismic transects (Cooke et al. 1992; Drummond et al. 1997; Goleby et al. 1998; Korsch et al. 2012): **a** east–west transect across the southern part of the North Australian Basin System (based on reinterpretation by R Korsch and M Doublier (unpublished) of 94MTI-01 (Drummond et al. 1997; Goleby et al. 1998)), **b** northeast-trending transect across the eastern margin of the North Australian Basin System showing the geometry of the Gidyea Structure (based on seismic line 07GA-IG1 (Korsch et al. 2012) in the northwest and extended to the south-west based on extrapolation of 94MTI-01 (Drummond et al. 1997; Goleby et al. 1998)), and **c** east–west transect across the southern part of the Northern Cordillera of western North America. Cross-section (**a**) equates to the southwestern part of 07GA-IG1 as extended to the southwest as a dashed line in Fig. 1c. Cross sections (**b**) and (**c**) equate to 94MTI-01 and Lithoprobe seismic traverses shown in Figs. 1c and 3c, respectively. Approximate location of significant nearby deposits have projected onto the transects. The Sullivan deposit projects just to the east of the eastern extent of (**c**). Symbols for deposit types are after Fig. 1

Major shale-hosted deposits in the Northern Cordillera of western North America are also associated with a (smaller amplitude) gradient in the 30-km upward-continued gravity image (Fig. 3d) as well as with gradients in the 15-, 50-, and 100-km upward-continued images (not shown), as also noted by Hayward and Paradis (2021). The relationship in this province differs from that in the Northern Australian Zinc Belt in two important ways. First, the gradient is not as strong as in the North Australian Zinc Belt, and second, the gradient has the opposite sense: the

Fig. 5 Conceptual plan, based on gravity data, showing the interpreted edges during the formation of the Calvert Superbasin. Location of major sediment-hosted zinc-lead and iron-oxide copper–gold deposits are shown
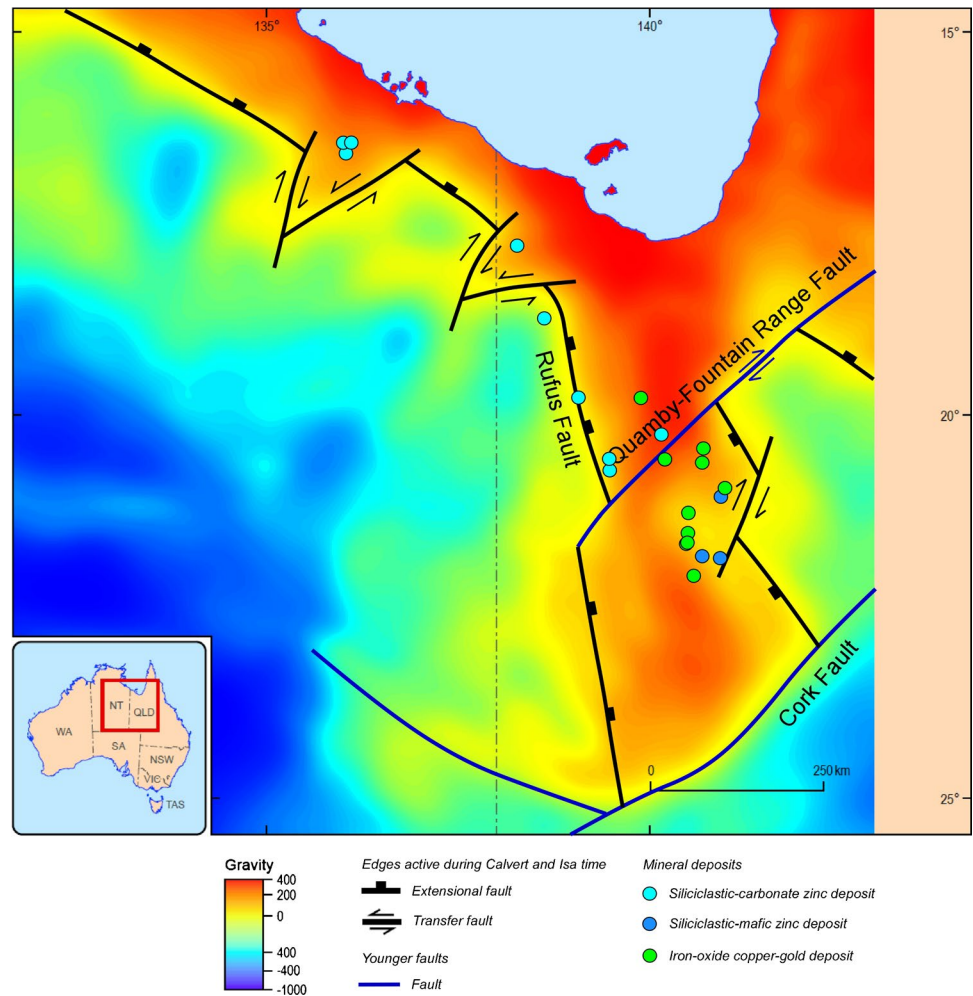
low-gravity zone is outboard relative to margin of the North American Craton.

Magnetotelluric data

Figure 1e shows the 36-km depth slice of the Northern Australia magnetotelluric electrical resistivity model (Duan et al. 2021). Unlike other mineral systems, in which deposits are associated with conductors (Heinson et al. 2018 for IOCG; Kirkby et al. 2022 for orogenic gold), the siliciclastic-carbonate zinc-lead deposits appear to be associated with a resistive zone between two more conductive zones. In the vicinity of Mount Isa, this resistivity anomaly trends north–south and broadly corresponds to the outcrop expression of the Kalkadoon-Leichhardt Belt, which is dominated by granites and gneisses. To the south of Mount Isa, this resistive zone trends toward the Cork Fault, although the lack of data in this region precludes determination of the southern extension of this zone. To the north of Mount Isa, the resistive corridor turns to the northwest and tracks toward the McArthur district, with all major siliciclastic-carbonate deposits, except Dugald River, located above the high resistivity anomaly.

To the east (northeast) and the west (southwest), the middle crust is significantly more conductive (Fig. 1e). Iron-oxide copper–gold and related epigenetic deposits of the Cloncurry district are spatially associated with the eastern high conductivity zone (Duan et al. 2021) as seen in other IOCG provinces such as Olympic Dam (Heinson et al. 2018). Siliciclastic-mafic zinc-lead deposits, such as Cannington and Pegmont, are also associated with this zone. The moderate to high conductive zone to the west of Mount Isa, however, is not associated with significant known mineral deposits of any type.

At the time of writing, insufficient magnetotelluric data have been collected in the Northern Cordillera to assess whether similar relationships between crustal electrical structure and the distribution of sediment-hosted zinc-lead deposits are present in that province.

Seismic reflection data

Figure 4a and b show interpreted sections from the North Australian Zinc Belt of transects 07GA-IG1 of the 2007 seismic reflection survey (Korsch et al. 2012) and 94MTI-01 of the 1994 survey (Goleby et al. 1998). These transects were chosen as they illustrate the crustal architecture of the North Australian Zinc Belt and cross gradients in μ, LAB depth, and gravity and magnetotelluric data as described above (locations shown in Fig. 1c). Figure 4a and b have been extended downwards to show the base of the lithosphere using depth contours of the LAB (Hoggard et al. 2020).

As shown in Fig. 4a and b, the southern part of the North Australian Zinc Belt comprises three crustal blocks that are divided by two north–south-trending, crustal-scale structures, the west-dipping Gidyea Structure[3] in the east and the steeply west-dipping Rufus Fault in the west. These structures are offset by the northwest-trending Quamby-Fountain Range Fault (Fig. 5), which offsets the gravity high in the 30-km upward-continued gravity image (Fig. 1d), as described above. Both the Gidyea Structure and the Rufus Fault are associated with offsets of the Moho, and both are considered major crustal boundaries (Korsch and Doublier 2016).

Figure 4c shows a Northern Cordillera cross-section from the western margin of the North American Craton in the east to Fraser River in the west (location shown in Fig. 3c) using the interpretation of Cook et al. (1992) for the composite Lithoprobe Northern Cordillera transect and the LAB depth model of Hoggard et al. (2020). Like the North Australian Zinc Belt transect, the Northern Cordillera section also indicates major crustal changes away from the margin of the North American Craton. The crust thins from east to west, accompanied by a major step in the Moho depth that also approximates the 170-km LAB depth contour. Similar to the North Australian Zinc Belt, the gradients seen in the lead isotope data and upward-continued gravity data, and distribution of shale-hosted zinc-lead deposits, appear to coincide with an edge, in this case the thinning of the North America Craton.

Discussion

Disparate datasets suggest that basin-hosted zinc-lead deposits in the North Australian Zinc Belt, the Northern Cordillera of western North America, and elsewhere in the world are associated with changes in the isotopic character, thickness,

_____
[3] Although Korsch et al. (2012) interpreted the Gidyea feature as suture, we have used the non-genetic term "structure" to describe this feature defined by the seismic data.

and physical properties (density and resistivity) of the crust and lithosphere. Data from the North Australian Zinc Belt suggest that these changes correspond to pre-existing boundaries between crustal blocks, whereas data from western North America suggest that deposits spatially coincide with the western boundary of the North American Craton.
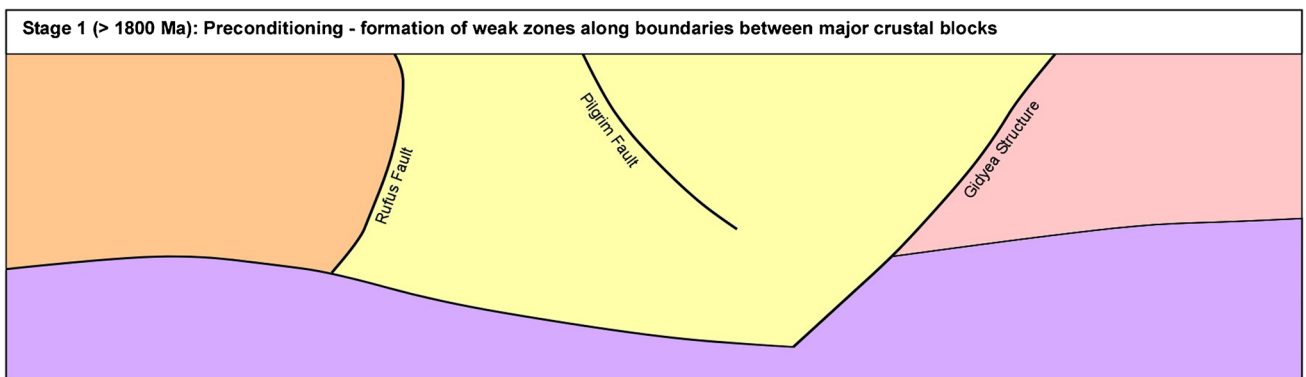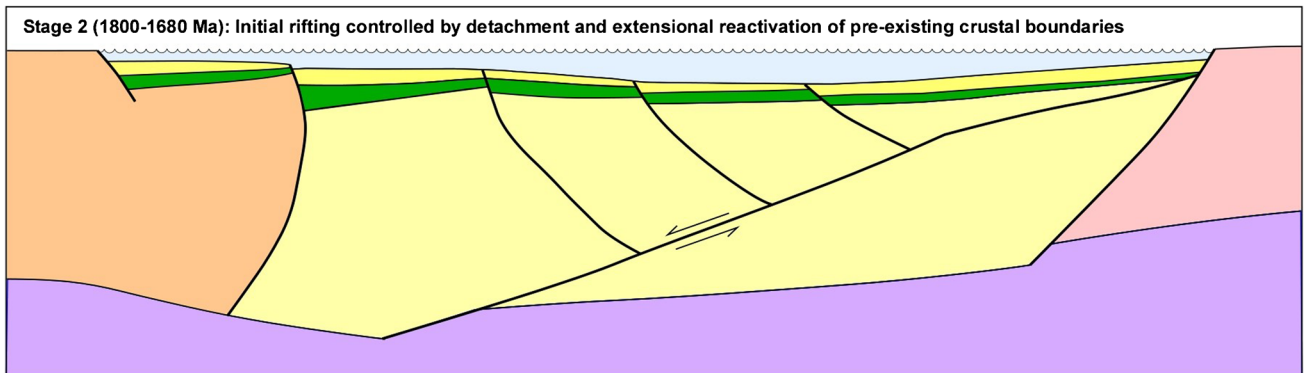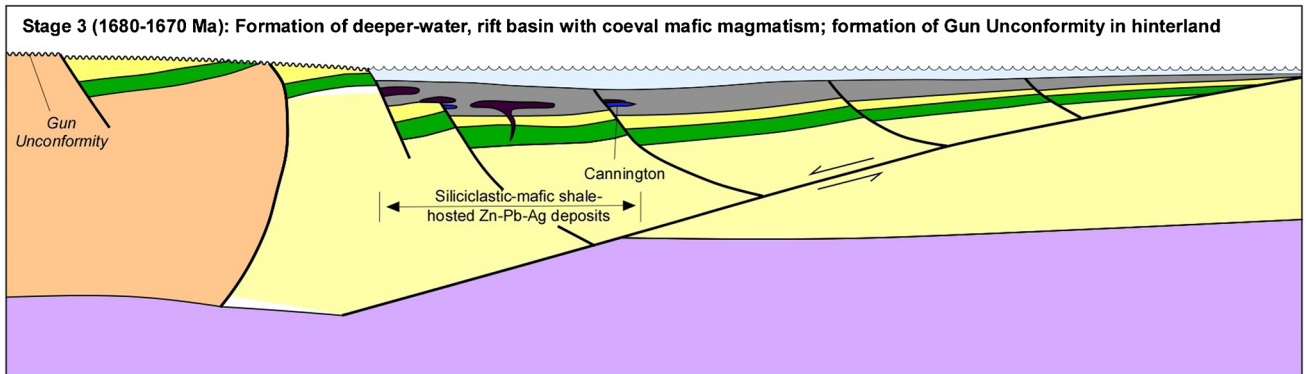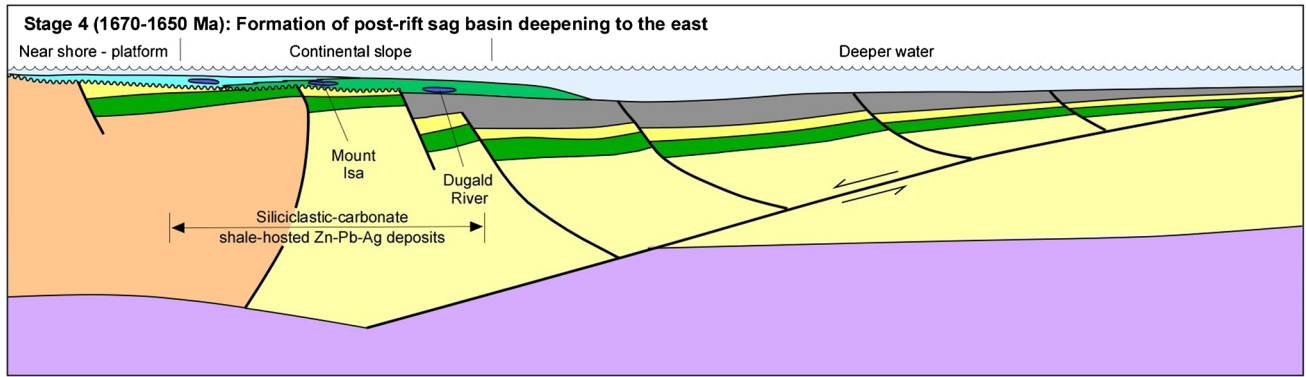
North Australian Zinc Belt

The present-day architecture of the southern part of the North Australian Zinc Belt consists of four major crustal blocks separated by three major structures (Figs. 4a and b and 5). The Gidyea Structure juxtaposes thicker, conductive crust of the Mount Isa Province to the west with thinner, resistive crust of the Kowanyama/Numil Seismic Province to the east (Fig. 4a). Within the Mount Isa Province, the east-dipping Pilgrim Fault juxtaposes conductive crust in the east from resistive crust to the west. Iron-oxide copper–gold and related deposits, and siliciclastic-mafic shale-hosted zinc-lead deposits, are mostly restricted to conductive Mount Isa crust, whereas siliciclastic-carbonate shale-hosted zinc-lead deposits are localized in the resistive corridor to the west. The Rufus Fault juxtaposes Mount Isa crust with thinner Aileron Province crust to the west (Fig. 4a). Lithospheric thickness decreases from west to east, with the 170-km LAB contour between the surface projection of the Gidyea Structure and the Rufus Fault.

In detail, trends determined from isotopic and gravity data, and the trend of the deposits themselves, cut at a broad scale the crustal-scale architecture described above. Moreover, the change in orientation to the northwest of the lead isotope, gravity, LAB-depth, and deposit trends and the resistive corridor are not obvious in the trends determined from surface geology and magnetic anomalies. In Fig. 5, we present a structural model that can account for the observed trends in multiple datasets and the distribution of mineral deposits using existing tectonic and basin architecture models for the North Australian Basin System (Neumann et al. 2009; Southgate et al. 2013; Gibson et al. 2016, 2018, 2020). This interpretation assumes that initiation of the Gidyea Structure and the Rufus Fault predated the formation of the North Australian Basin System and that their geometry strongly influenced the architecture of the North Australian Basin System. Gibson et al. (2008, 2012) argued that the evolution of the basin system between ca. 1790 and ca. 1620 Ma was strongly influenced by east-northeast–west-southwest- to northeast–southwest-directed extension associated with the rifting of Laurentia from the North Australian Craton. Korsch et al. (2012) argued that the Gidyea Structure formed before ca. 1850 Ma.

Our interpretation (Fig. 5) conceptually involves the formation of a basin during northeast-southwest extension and is based mostly on gravity data but uses all datasets

Stage 4 (1670-1650 Ma): Formation of post-rift sag basin deepening to the east

Near shore - platform
Continental slope
Deeper water

Mount Isa

Dugald River

Siliciclastic-carbonate shale-hosted Zn-Pb-Ag deposits

Stage 3 (1680-1670 Ma): Formation of deeper-water, rift basin with coeval mafic magmatism; formation of Gun Unconformity in hinterland

Gun Unconformity

Cannington

Siliciclastic-mafic shale-hosted Zn-Pb-Ag deposits

Stage 2 (1800-1680 Ma): Initial rifting controlled by detachment and extensional reactivation of pre-existing crustal boundaries

Stage 1 (> 1800 Ma): Preconditioning - formation of weak zones along boundaries between major crustal blocks

Rufus Fault

Pilgrim Fault

Gidyea Structure

Legend:

- Siliciclastic-carbonate shale-hosted zinc-lead-silver deposits
- Siliciclastic-mafic shale-hosted zinc-lead-silver deposits
- Isa Superbasin: Siliciclastic-dominated lithofacies — fluviatile to deep marice sandstone and siltstone
- Isa Superbasin: Carbonate-dominated lithofacies — dolostone with minor limestone
- Gun unconformity
- Calvert Superbasin: dominantly deeper-marine siliciclastic rocks (gray) with mafic sills and possible lavas (violet)
- Calvert Superbasin: dominantly shallow-marine siliciclastic and carbonate rocks with lesser mafic and felsic volcanic rocks and sills
- Leichhardt Superbasin: continental tholeiites, fluvial to lacustrine siliciclastic and minor carbonate rocks
- Numil-Kowanyama Province
- Mount Isa Province
- Aileron Province
- Lithospheric mantle

Springer

◄**Fig. 6** Conceptual model of shale-hosted zinc-lead mineral systems (based on the North Australia Zinc Belt in the vicinity of Mount Isa) showing relationship of these systems to crustal edges: **a** stage 1, preconditioning; **b** stage 2, initial rifting; **c** stage 3, formation of rift basin; and **d** formation of sag basin

described herein. Three sets of faults controlled the geometry of the basin: (1) newly formed, northwest-striking extensional faults; (2) north-trending trans-tensional faults that reactivated pre-existing crustal-scale faults such as the Gidyea Structure and Rufus Fault; and (3) deep-seated northeast-striking transfer faults. In this interpretation, the edges created by the extensional and trans-tensional faults controlled the sedimentary facies architecture of the North Australian Basin System (cf. Southgate et al. 2013; Fig. 2). Smaller-scale extensional and transfer faults, developed on this large-scale architecture, likely compartmentalized local sub-basin development (Gibson et al. 2016, 2018). The complex, small-scale *en echelon* distribution pattern of lead isotope data, reflected by μ values (Fig. 1b), likely reflects the development of such basins, and the re-entrants in gravity anomalies in the McArthur River and Walford Creek districts (Fig. 1d) may similarly reflect sub-basin development.

Northern Cordillera

The present-day Northern Cordillera consists of a series of allochthonous and para-autochthonous terranes accreted onto the western margin of the North American Craton. This margin is irregular with many sub-basin embayments and basement-cored promontories controlled by local extensional and transform faults. Changes in the width and thickness of sedimentary rocks within these sub-basins reflect asymmetric extension (Thomas 1977; Lund 2008; Colpron and Nelson 2021). The broad-scale breaks in both upward-continued gravity (Fig. 3c) and μ data (Fig. 3b) likely reflect this margin, but the complex, smaller-scale patterns in μ reflect the development of sub-basins along this margin.

Shale-hosted zinc-lead deposits in the Northern Cordillera occur along linear trends that may be related to basement structures that originated during rifting along the margin of the North American Craton (Lund 2008; McMechan 2012). These structures influenced the geometry of the rift system and provided conduits for magmas and/or hydrothermal fluids. Northwest-striking asymmetric extensional segments and crustal thinning in the region are subdivided by northeast-striking transform and transfer segments.

Asymmetric extension produced margins, or edges, that mark changes in the character of both basin and basement. Lower-plate margins (i.e., Selwyn Basin and Mackenzie Platform in Yukon) are marked by the thinning of continental crust, subsidence (producing thick sag basins), and rotated crustal blocks. Upper-plate margins (i.e., south of the Laird line up to the Vulcan Low-St. Marie-Moyie transform zone; Fig. 1 of Lund et al. 2010) are characterized by limited crustal thinning and narrower continental margins (Thomas 1993, 2006).

Most of the largest shale-hosted zinc-lead deposits in the Northern Cordillera are located in the segment associated with the lower plate margin, including those in the Selwyn Basin and Mackenzie Platform. Another group of important deposits, including Sullivan, is in southern British Columbia where the Vulcan Low-St. Marie-Moyie transform zone, a deep and old crustal structure within the North American Craton (Hoffman 1988), defines an upper-plate margin. Northeast-striking transform and transfer faults played important roles on sedimentation, intrusion, deformation, and mineralization (Lund et al. 2010), and many sediment-hosted deposits are located along these faults (e.g., Sullivan located along the Vulcan Low-St. Marie-Moyie structure).

Like the North Australian Zinc Belt, major shale-hosted zinc-lead deposits appear to be associated with cratonic edges, determined both geologically and using lead isotope data, the depth of the LAB and gravity data. It also appears that local-scale features, such as basement structures, also were an important control on the distribution of the deposits. Similar to the North Australian Zinc Belt, some of the fine-scale complexity in μ variations may reflect these structures.

Edges—fundamental controls on the distribution of shale-hosted zinc-lead deposits

Continental or cratonic edges, which can be outlined using a range of isotopic and geophysical datasets, appear to have exerted a large influence on the distribution of shale-hosted zinc-lead deposits. In the North Australian Zinc Belt, the older (ca. 1680 Ma) siliciclastic-mafic deposits occur outboard of the platform edge in deep-water turbiditic successions that formed during the early rift phase of basin development. In contrast, the younger (ca. 1665–1575 Ma), siliciclastic-carbonate deposits formed along or inboard of the edge as the basin continues to develop. This distribution of both deposit types is shown schematically in Fig. 2. In the Northern Cordillera, the relationship is broadly similar. Figure 6 presents an evolutionary model for the North Australian Zinc Belt illustrating how edges have controlled the metallogeny of this province. Figure 7 shows the general relationships of deposits to edges and geochemical and geophysical proxies of edges.

Architecture of the North Australian Zinc Belt

Figure 6 shows conceptually how a basin-hosted tectono-metallogenic system may have evolved, based on geometric relationships in the southern part of the North Australian Zinc Belt. In this model, the basement architecture of the
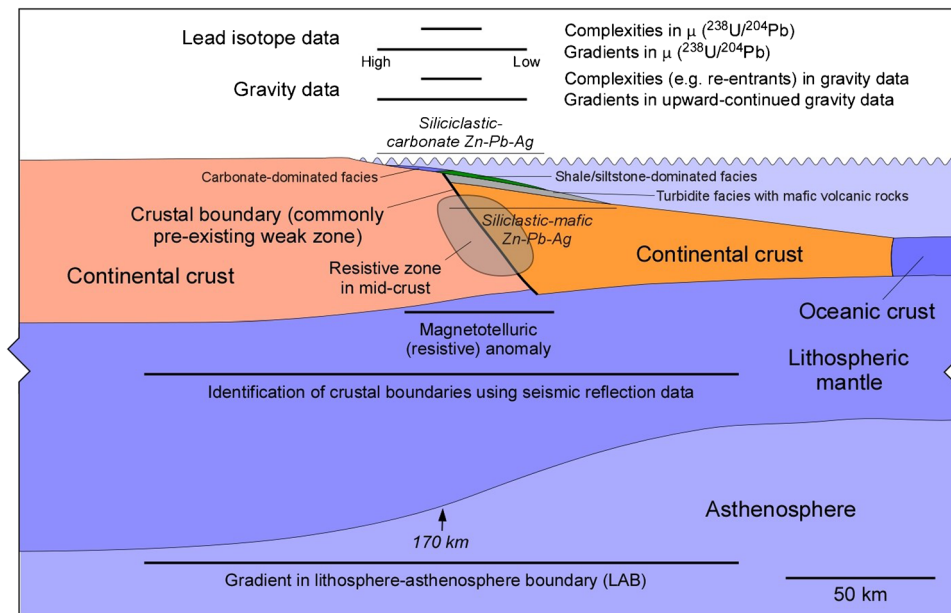
Fig. 7 Schematic diagram showing the control of cratonic edges on the distribution of shale-hosted zinc deposits (modified after Huston et al. 2016). The relative resolution of different datasets discussed in the text in defining prospective basins and zones within basins for these deposits is shown. The diagram is generalized, and the characteristics and utility of the datasets presented vary between basins. Other factors that should be considered in basin analysis include age, paleoenvironmental characteristics of the basin (e.g., paleolatitude and/or evidence of evaporites), tectonic triggers (e.g., out-of-area structural and/or tectonic events as indicated by bends in paleomagnetic apparent polar wander paths or local structural events), the presence of and evidence for leaching of source rocks (e.g., mafic volcanic rocks and certain turbiditic sedimentary rocks), and the presence of trap rocks (mainly carbonaceous and dolomitic shale/siltstone, but in some cases, dolostone breccia)

zinc belt is inherited from pre-existing major crustal boundaries and/or structures, including the Gidyea Structure and the Rufus and Pilgrim faults (Fig. 6a). These faults separate domains with different physical (i.e., density, seismic character, and resistivity structure) and isotopic properties, and, as such, represent the edges of major cratonic blocks that controlled later basin evolution and metallogenesis.

At ca. 1790 Ma, extension initiated, leading to deposition of the Leichhardt Superbasin and the basal part of the Calvert Superbasin over the following 140 Myr (Fig. 6b). Although shown simply as an extensional basin with edges defined by pre-existing boundary faults, in detail this early extension may have involved formation of core complexes and other more complex extensional geometries (e.g., Gibson et al. 2008). Rocks deposited at this time are mainly tholeiitic mafic volcanic rocks, lacustrine and shallow marine sandstone and other siliciclastic rocks, and minor carbonate rocks. This deposition continued to ca. 1680 Ma (Fig. 6c), at which time a deeper rift basin formed in the eastern part of the Calvert Superbasin, partly controlled by the early formed structural architecture, particularly the Pilgrim Fault. This depositional system was dominated by turbiditic, siliciclastic rocks but included mafic volcanic rocks. Siliciclastic-mafic deposits such as Cannington formed at this time. The deposition of this rift basin corresponded in time with erosion and the development of the regional Gun unconformity in the western part of the North Australian Basin System (Neumann et al. 2009; Southgate et al. 2013).

Rifting ceased at ca. 1670–1665 Ma, and the basin system went into a sag phase (Fig. 6d). At this time, magmatism became very minor and sedimentation involved deposition of siliciclastic- and carbonate-dominated facies that changed laterally from the shelf outward and eastward into deeper-water sediments (Southgate et al. 2013: Figs. 2 and 6d). The transition from the shelf into deeper water in this sedimentary system was likely controlled by the edges formed during earlier extension. This transition from carbonate-rich successions on the platform to calcareous/dolomitic shale successions in deeper water was important for the development of mineral systems that form siliciclastic-carbonate shale-hosted zinc-lead deposits (e.g., Emsbo et al. 2016). These deposits formed throughout much of the sedimentary system, from carbonate-rich succession on the platform (e.g., McArthur River and Lady Loretta) to successions where carbonate is not as dominant (e.g., Mount Isa, Dugald River).

Although the model presented in Fig. 6 does not apply directly to the Northern Cordillera, the presence of an edge, as indicated in μ variations and variations in the LAB and in gravity data, had a strong control on the distribution of most shale-hosted zinc-lead deposits in this orogen (Fig. 3).

Moreover, the range in age of the deposits suggest that this margin was long-lived, with mineralizing events occurring at ca. 1475 Ma, ca. 560 Ma, ca. 520 Ma, ca. 440 Ma, and ca. 380–365 Ma.

Controls on siliciclastic-mafic and siliciclastic-carbonate shale-hosted deposits

The spatial association of the Cannington deposit with amphibolite (Wright et al. 2017), interpreted as a mafic volcanic rock or sill, and the presence of mafic sills and dikes within the host Soldiers Cap Group (Derrick et al. 1976; Beardsmore et al. 1988; Gibson et al. 2018), indicates significant coeval magmatism in a relatively deep rift basin. It is likely that the edges, as discussed above, controlled the development of this basin. Moreover, lithospheric thinning and mafic magmatism associated with rifting likely resulted in a high heat flow, which drove the circulation of relatively hot, reduced ore fluids that deposited metals in the shallow subsurface below the seafloor (Cooke et al. 2000; Huston et al. 2006; Wright et al. 2017). The metal source was likely mafic volcanic rocks or immature, turbiditic siliciclastic rocks within the rift basin.

In contrast, siliciclastic-carbonate zinc-lead deposits are thought to have formed from lower temperature, oxidized ore fluids (Cooke et al. 2000; Huston et al. 2006). Modeling by Hoggard et al. (2020) has suggested that thicker subcontinental lithospheric mantle and crust insulates overlying basins from hot asthenosphere mantle during mild to moderate rifting, resulting in lower thermal gradients within rift basins. In addition, thicker basins develop during rifting of the thick and buoyant lithosphere. These two factors are combined to produce voluminous sediments in basins having lower-temperature brines, which, if oxidized, can be highly efficient at transporting base metals (Cooke et al. 2000; Huston et al. 2016). Moreover, the mafic volcanic rocks deeper in the basin are ideal source rocks for zinc (Cooke et al. 1998, 2000; Champion et al. 2020).

Cratonic edges juxtapose contrasting geological and tectonic environments in space and time—environments that provide essential components (architecture, fluids, fluid pathways, source rocks, and traps) for both siliciclastic-mafic and siliciclastic-carbonate zinc mineral systems (Fig. 7). In this study, we have demonstrated that cratonic edges can be mapped using diverse datasets—lead isotopes, surface-wave tomography, gravity, seismic reflection, and magnetotelluric data—and that the locations of deposits correspond closely with the mapped edges. Moreover, these edges have persisted and localized deposits for long periods of geological time. In the North Australian Zinc Belts, deposits formed along the edge for over 100 Myr, and in the Northern Cordillera, deposits formed along the edge at ca. 1475 Ma and for over 100 Myr in the Paleozoic.

Although we emphasized the relationship of shale-hosted zinc-lead deposits with the large-scale edges (Fig. 7), in detail, the locations of many deposits seem to be controlled by second-order features along these large-scale boundaries. In particular, the Walford Creek deposit and those in the McArthur district in the North Australian Zinc Belt are associated with embayments in the 30-km upward-continued gravity image (Fig. 1d); some deposits in the Northern Cordillera are associated with complexities in μ patterns (Fig. 3b). The McMillan Pass and Howards Pass districts are associated with an embayment in the gravity data (see also Hayward and Paradis 2021). These relationships suggest that anomalous, smaller-scale features in isotopic, gravity, and other datasets may be useful in defining more prospective zones along the larger-scale margins, although more detailed data are required to test this concept.

In the North Australian Zinc Belt and to a lesser extent in the Northern Cordillera, most deposits are localized where edges identified by all datasets coincide (Fig. 7). Outside of these areas of coincidence, major deposits are not known, although much of the area is covered by younger basins, at least in the North Australian Zinc Belt. Outside of the areas of known mineralization, locations of edges, as determined from the different datasets, diverge, which raises the question: which dataset provides the best vector for targeting at different scales? More data and examples are required to resolve this question.

Lastly, evidence presented by Young (2004) for the Red Dog tectonic plate, which hosts the Red Dog district, and Hayward and Paradis (2021) for the Selwyn Basin, which hosts the MacMillan Pass and Howards Pass districts, suggests that some basins that contain shale-hosted zinc deposits have been transported significant distances relative to basement by post-basin thrusting. This inferred post-ore tectonic displacement may account for local divergence of deposits from geophysical features identified in the basement and underlying mantle (e.g., the LAB 170-km contour: Hayward and Paradis 2021) and the location of deposits. Although these deeper features provide criteria to identify mineralized provinces or basins at the global scale, more precise location information may be provided by datasets that directly map the characteristics of the host basin and are independent of post-mineral translation. These datasets include lead isotope data and more detailed gravity data.

Other criteria bearing on basin fertility

Global reviews on the characteristics and temporal distribution of basin-hosted zinc-lead deposits (Leach et al. 2005, 2010; Wilkinson 2014) provide additional insights on important controls of these deposits. The oldest major basin-hosted zinc-lead deposit has an age of ca. 1800 Ma (Rampura-Agucha in India; Deb and Thorpe 2004) and was

succeeded by a major period of deposit formation, including deposits from the North Australian Zinc Belt and the Northern Cordillera, at ca. 1800–1475 Ma. Formation of this cluster followed the development of an oxidized, upper layer of the ocean (Farquhar et al. 2010), which allowed, for the first time, the development of oxidized fluids essential for hydrothermal transport of metals in cool basins that formed over thickened lithosphere. Hence, a basin age younger than ca. 1800 Ma can be used as an additional criterion to define prospective basins.

Information on paleoenvironments at the time of mineralization can also refine the search space. Based on data for Phanerozoic deposits, Leach et al. (2005) suggested that virtually all basin-hosted zinc-lead deposits formed within 30° (mostly 10–30°) from the equator, the equivalent of modern desert belts. Paleomagnetic data suggest that the North Australian Zinc Belt was within 40° of the equator at the time of zinc-lead mineralization (Idnurm 2000). These data indicate that an arid littoral environment, critical for the formation of evaporative brines, is essential to form basin-hosted zinc-lead deposits. In addition to paleomagnetic data, the presence of evaporites, evaporitic textures, evaporitic minerals, or mineral or textural pseudomorphs of evaporitic minerals within the host succession may also indicate favorable basins (Davidson and Dashlooty 1993; Czarnota et al. 2020).

Idnurm (2000) showed that many of the major siliciclastic-carbonate zinc-lead deposits in the North Australian Zinc Belt are temporally associated with bends in the apparent polar wander path of the North Australian Craton. The 1635–1645 Ma McArthur River and Lady Loretta deposits correspond in time not only to a major bend in this path, but also to the Liebig Orogeny (Scrimgeour et al. 2005) on the southern margin of the North Australian Craton and the Riversleigh Tectonic Event within the North Australian Basin System. Hence, the trigger of fluid flow in the North Australian Zinc Belt may be regional or out-of-area structural-tectonic events that are apparent in the paleomagnetic and/or structural history of the North Australian Craton. Similarly, the formation of the Sullivan deposit (~ 1475 Ma; Slack et al. 2020) coincides in time with a major bend on the North American apparent polar wander path (Elston et al. 2002; Leach et al. 2010), and the Howards Pass (~ 442 Ma; Kelley et al. 2017) and Red Dog (~ 338 Ma; Morelli et al. 2004) deposits are broadly associated with flexures in the Paleozoic North American polar wander path (Cocks and Torsvik 2011). This information may provide time constraints that can further refine the exploration search space in those regions.

Cooke et al. (1998) and Champion et al. (2020) have demonstrated that zinc and copper in many basaltic rocks from the Leichhardt and Calvert superbasins were depleted in association with regional chlorite-, K-feldspar-, and/or hematite-bearing alteration assemblages. Preliminary data suggest that copper leaching may be associated with demagnetization of the basalt (Champion et al. 2020). The presence of such altered rocks is an additional characteristic of a fertile basin. Insufficient data are available to test this concept in basins developed at various times along the margin of the North American Craton.

All significant siliciclastic-carbonate zinc-lead deposits in the North Australian Zinc Belt are hosted by carbonaceous and dolomitic siltstone lenses within carbonate- and/or sandstone-rich successions (Large et al. 2005; Czarnota et al. 2020). These fine-grained rocks most likely formed in restricted, deeper-water depocenters and acted as redox traps to metals deposited from oxidized ore fluids, either epigenetically (Broadbent et al. 1998; Spinks et al. 2021), diagenetically in the shallow subsurface (Williams 1978; Kelley et al. 2004a,b; Gadd et al. 2016, 2017), or syngenetically on the sea floor (Carne and Cathro 1982; Goodfellow et al. 1993; Large et al. 2005). The presence of these fine-grained rocks enhances the fertility of basins for siliciclastic-carbonate zinc-lead deposits (although not for some other basin-hosted deposits); hence, the identification of spatial and temporal positions of these depocenters can further constrain the search space.

Our results indicate that other disparate datasets, including stratigraphic, geochemical, and paleomagnetic data, may further refine spatial and/or temporal domains within basin systems that are most prospective. Moreover, it is possible that potential field, facies architecture, and, possibly, lead isotope data can be used to identify prospective domains at the district scale.

Conclusions

Although cartoon-like diagrams of basin-hosted mineral systems (e.g., Large 1980; Leach et al. 2005, 2010; Huston et al. 2016) have long suggested that these deposits form along the edges of continental blocks on passive margins, this study shows that data such as ore lead isotope analyses, surface-wave tomography converted to temperature, upward-continued gravity, and, possibly, low- to mid-crustal magnetotelluric data can map the distribution of these cratonic margins (Fig. 7), even if the margins have been involved in later collisional events. The surface-wave tomography data, in particular, suggest that continental margins are associated with thicker lithosphere; seismic-reflection data further suggest that the formation of passive margins localized along pre-existing crustal boundaries are more prospective for major and world-class shale-hosted zinc deposits. These features appear to be a first-order control on basins that are highly fertile for basin-hosted mineral deposits and can be used as exploration guides in area selection.

Importantly, there are ways to screen more prospective from less prospective basins and to determine the most prospective parts of prospective basins. Our results and previous data suggest that more prospective basins are (1) no older than ca. 1800 Ma, (2) formed within 30–40° of the equator, (3) overlap in age with bends in apparent polar wander paths, and (4) overlap in space with cratonic edges identified using variations in radiogenic isotopes and geophysical data (Fig. 7). The most prospective parts of basins are indicated by the location of cratonic edges, perturbations in these edges, sedimentary facies changes in time and in space, evidence for the presence of evaporites in the sedimentary succession, and existence of extensive syn-basin faults.

References

Bain JHC, Heinrich CA, Henderson GAM (1992) Stratigraphy, structure, and metasomatism of the Haslingden Group, east Moondarra area, Mount Isa: a deformed and mineralized Proterozoic multistage rift-sag sequence. Bur Min Res BMR Bull 243:125–136

Barrie CT, Hannington MD (1999) Classification of volcanic-associated massive sulfide deposits based on host-rock composition. Rev Econ Geol 8:1–11

Beardsmore TJ, Newberry SP, Laing WP (1988) The Maronan Supergroup: an inferred early volcanosedimentary rift sequence in the Mount Isa Inlier, and its implications of ensialic rifting in the Middle Proterozoic of northwest Queensland. Precam Res 40(41):487–507

Box SE, Karl SM, Jones JV III, Bradley DC, Haeussler PJ, O'Sullivan PB (2019) Detrital zircon geochronology along a structural transect across the Kahiltna assemblage in the western Alaska Range: implications for emplacement of the Alexander-Wrangellia-Peninsular terrane against North America. Geosphere 15:1774–1808

Broadbent GC, Myers RE, Wright JV (1998) Geology and origin of shale-hosted Zn-Pb-Ag mineralization at the Century deposit, northwest Queensland, Australia. Econ Geol 93:1264–1294

Carne RC, Cathro RJ (1982) Sedimentary exhalative (SEDEX) zinc-lead-silver deposits, northern Canadian Cordillera. CIM Bull 75(840):66–78

Carr GR, Denton GJ, Korsch MJ, Gardner BL, Parr JM, Andrew AS, Whitford DJ, Wyborn LAI, Sun S-S (2001) User friendly isotope technologies in mineral exploration: Pb isotope applications, Northern Australian Proterozoic basins. CSIRO Rep 713C, 127 p

Champion DC, Huston DL, Bastrakov E, Siegel C, Thorne J, Gibson GM, Hauser J (2020) Alteration of mafic igneous rocks of the southern McArthur Basin: comparisons with the Mount Isa region and implications for basin-hosted base metal deposits. Exploring for the future: extended abstracts, Geoscience Australia, Canberra, https://doi.org/10.11636/134206

Champion DC, Huston DL (2016) Radiogenic isotopes, ore deposits and metallogenic terranes: novel approaches based on regional isotopic maps and the mineral systems concept. Ore Geol Rev 76:229–256

Church SE, Delevaux MH, Gray JE (1987) Pb-isotope data base for sulfides from Alaska. US Geol Survey Open-File Rept 87–259

Clowes RM (1990) LITHOPROBE: a scientific update-new images of the continental crust. Tectonophys 173:639

Cocks LRM, Torsvik TH (2011) The Palaeozoic geography of Laurentia and western Laurussia: a stable craton with mobile margins. Earth-Sci Rev 106:1–51

Colpron M, Nelson JL (2021) Northern Cordillera: Canada and Alaska. Encyclopedia of Geology, Elsevier Ltd,. https://doi.org/10.1016/B0-12-369396-9/00401-9

Colpron M, Nelson JL, Murphy DC (2006) A tectonostratigraphic framework for the pericratonic terranes of the northern Canadian Cordillera. Geol Assoc Can Spec Pap 45:1–23

Colpron M, Nelson JL (2020) A digital atlas of terranes for the Northern Cordillera. Yukon Geol Survey digital atlas. https://data.geology.gov.yk.ca/Compilation/2#DescriptionTab

Coney PJ, Jones DL, Monger JWH (1980) Cordilleran suspect terranes. Nature 288:329–333

Cook FA (1995) The southern Canadian Cordillera transect of LITHO-PROBE. Can J Earth Sci 32:1483–1824

Cook FA, Varsek JL, Clowes RM, Kanasewich ER, Spencer CS, Parrish RR, Brown RL, Carr SD, Johnson BJ, Price RA (1992) Lithoprobe crustal reflection cross section of the southern Canadian Cordillera, 1, Foreland thrust and fold belt to Fraser River fault. Tectonics 11:12–35

Cook FA, Erdmer P, van der Velden AJ (2012) The evolving Cordilleran lithosphere. Geol Assoc Canada Spec Paper 49:1–39

Cooke DR, Bull SW, Donovan S, Rogers JR (1998) K-metasomatism and base metal depletion in volcanic rocks from the McArthur Basin, Northern Territory: implications for base metal mineralization. Econ Geol 93:1237–1263

Cooke DR, Bull SW, Large RR, McGoldrick PJ (2000) The importance of oxidized brines for the formation of Australian Proterozoic stratiform sediment-hosted Pb-Zn (Sedex) deposits. Econ Geol 95:1–18

Czarnota K, Hoggard MJ, Richards FD, Teh M, Huston DL, Jaques AL, Ghelichkhan S (2020) Minerals on the edge: sediment-hosted base metal endowment above steps in lithospheric thickness. Exploring for the future: extended abstracts, Geoscience Australia, Canberra, https://doi.org/10.11636/134991

Davidson GJ, Dashlooty SA (1993) The Glyde Sub-basin: a volcaniclastic-bearing pull-apart basin coeval with the McArthur River base-metal deposit, Northern Territory. Aust J Earth Sci 40:527–543

Deb M, Thorpe RI (2004) Geochronological constraints in the Precambrian geology of Rajasthan and their metallogenic implications. Sediment-hosted lead-zinc sulphide deposits—attributes and models of some major deposits in India, Australia and Canada. New Delhi, Narosa Publishing House, 246–263

Derrick GM, Wilson IH, Hill RM (1976) Revision of stratigraphic nomenclature in the Precambrian of northwestern Queensland. V. Soldiers Cap Group. Queensland Gov Min J 77:600–604

Drummond BJ, Goleby BR, Goncharov AG, Wyborn LAI, Collins CDN, MacCready T (1997) Crustal-scale structures in the Proterozoic Mount Isa Inlier of north Australia: their seismic response and influence on mineralisation. Tectonophysics 288:43–56

Duan J, Kyi D, Jiang W (2021) Electrical resistivity structures and mineral prospectivity from exploring for the future AusLAMP data (2016–2019) in Northern Australia. Geosci Aust Rec 2021/21. https://doi.org/10.11636/Record.2021.021

Duncan RJ, Stein HJ, Evans KA, Hitzman MW, Nelson EP, Kirwin DJ (2011) A new geochronological framework for mineralization and alteration in the Selwyn-Mount Dore corridor, Eastern Fold Belt, Mount Isa Inlier, Australia: genetic implications for iron oxide copper-gold deposits. Econ Geol 106:169–192

Elston DP, Enkin RJ, Baker J, Kisilivsky DK (2002) Tightening the belt: Paleomagnetic-stratigraphic constraints on deposition, correlation, and deformation of the Middle Proterozoic (ca. 1.4 Ga) Belt-Purcell Supergroup, United States and Canada. Geol Soc Am Bull 114:619–638

Emsbo P, Seal RR, Breit GN, Diehl SF, Shah AK (2016) Sedimentary exhalative (sedex) zinc-lead-silver deposit model. US Geol Survey Sci Invest Rept 2010–5070–N, 57

Farquhar J, Wu N, Canfield D, Oduro H (2010) Connections between sulfur cycle evolution, sulfur isotopes, sediments and base metal sulfide deposits. Econ Geol 105:509–534

Fernandes NA, Gleeson SA, Magnall JM, Creaser RA, Martel E, Fischer BJ, Sharp R (2017) The origin of Late Devonian (Frasnian) stratiform and stratabound mudstone-hosted barite in the Selwyn Basin, Northwest Territories, Canada. Marine Petrol Geol 85:1–15

Fishwick S, Rawlinson N (2012) 3-D structure of the Australian lithosphere from evolving seismic datasets. Aust J Earth Sci 59:809–826

Gadd M, Layton-Matthews D, Peter J, Paradis S (2016) The world-class Howard's Pass Zn-Pb SEDEX district, Selwyn basin Yukon. Part 1: trace element compositions of pyrite record input of hydrothermal, diagenetic and metamorphic fluids to mineralization. Mineral Deposita 51:319–342

Gadd M, Layton-Matthews D, Peter J, Paradis S (2017) The world-class Howard's Pass SEDEX Zn-Pb district, Selwyn Basin Yukon. Part 2: the roles of thermochemical and bacterial sulfate reduction in metal fixation. Mineral Deposita 52:405–419

Geological Survey of Canada (2017) Geoscience data repository for geophysical data, gravity, point data. Natural Resources Canada, http://gdr.agg.nrcan.gc.ca/gdrdap/dap/search-eng.php

Gibson GM, Rubenach MJ, Neumann NL, Southgate PN, Hutton LJ (2008) Syn- and post-extensional tectonic activity in the Palaeoproterozoic sequences of Broken Hill and Mount Isa and its bearing on reconstructions of Rodinia. Precam Res 166:350–369

Gibson GM, Henson PA, Neumann NL, Southgate PN, Hutton LJ (2012) Paleoproterozoic-earliest Mesoproterozoic basin evolution in the Mount Isa region, northern Australia and implications for reconstructions of the Nuna and Rodinia supercontinents. Episodes 34:131–141

Gibson GM, Meixner AJ, Withnall IW, Korsch RJ, Hutton LJ, Jones LEA, Holzschuh J, Costelloe RD, Henson PA, Saygin E (2016) Basin architecture and evolution in the Mount Isa mineral province, northern Australia: constraints from deep seismic reflection profiling and implications for ore genesis. Ore Geol Rev 76:414–441

Gibson GM, Hutton LJ, Holzschuh J (2017) Basin inversion and supercontinent assembly as drivers of sediment-hosted Pb–Zn mineralization in the Mount Isa region, northern Australia. J Geol Soc London 174:773–786

Gibson GM, Champion DC, Withnall IW, Neumann NL, Hutton LJ (2018) Assembly and breakup of the Nuna supercontinent: geodynamic constraints from 1800 to 1600 Ma sedimentary basins and basaltic magmatism in northern Australia. Precam Res 313:148–169

Gibson GM, Champion DC, Huston DL, Withnall IW (2020) Orogenesis in Paleo-Mesoproterozoic eastern Australia: a response to arc-continent and continent-continent collision during assembly of the Nuna Supercontinent. Tectonics 39:e2019TC005717. https://doi.org/10.1029/2019TC005717

Goleby BR, MacCready T, Drummond BJ, Goncharov A (1998) The Mount Isa geodynamic transect – crustal implications. Amer Geophy Union Geodyn Series 26:109–118

Goodfellow WD (2007) Base metal metallogeny of the Selwyn Basin, Canada. Geol Assoc Canada Min Deposits Div Spec Paper 5:553–579

Goodfellow GD, Lydon JW, Turner RJW (1993) Geology and genesis of stratiform sediment-hosted (SEDEX) zinc-lead-silver sulphide deposits. Geol Assoc Canada Spec Paper 40:201–251

Hammer PTC, Clowes RM, Cook FA, van der Velden AJ, Vasudevan K (2010) The Lithoprobe trans-continental lithospheric cross sections: imaging the internal structure of the North American continent. Can J Earth Sci 47:821–857

Hampton BA, Ridgway KD, Gehrels GE (2010) A detrital record of Mesozoic island arc accretion and exhumation in the North American Cordillera: U–Pb geochronology of the Kahiltna basin, southern Alaska. Tectonics 29:TC4015. https://doi.org/10.1029/2009TC002544

Hayward N (2015) Geophysical investigation and reconstruction of lithospheric structure and its control on geology, structure, and mineralization in the Cordillera of northern Canada and eastern Alaska. Tectonics 34:2165–2189

Hayward N, Paradis S (2021) Geophysical reassessment of the role of ancient basement structures on the development of western Laurentia and Selwyn Basin, Yukon and NWT, Canada. Can J Earth Sci 58:1283–1300. https://doi.org/10.1139/cjes-2021-0003

Heinson G, Didana Y, Soeffky P, Thiel S, Wise T (2018) The crustal geophysical signature of a world-class magmatic mineral system. Sci Rept 8:10608. https://doi.org/10.1038/s41598-018-29016-2

Hejrani B, Hassan R, Gorbatov A, Sambridge M, Hawkins R, Valentine A, Czarnota K, Zhao J (2020) Ambient noise tomography of Australia: application to AusArray deployment. Exploring for the Future: Extended Abstracts, Geoscience Australia, Canberra, https://doi.org/10.11636/135130

Hobbs BE, Ord A, Archibald NJ, Walshe JL, Zhang Y, Brown M, Zhao C (2000) Geodynamic modelling as an exploration tool. Aust Inst Mining Metall Publ Series 2:34–49

Hoffman PF (1988) United plates of America: the birth of a craton. Ann Rev Earth Planet Sci 16:543–603

Hoggard MJ, Czarnota K, Richards FD, Huston DL, Jaques AL, Ghelichkhan S (2020) Global distribution of sediment-hosted metals controlled by craton edge stability. Nature Geosci 13:504–510

Hollis SP, Doran AL, Menuge JF, Daly JS, Guven J, Piercey SJ, Cooper M, Turner O, Unitt R (2019) Mapping Pb isotope variations across Ireland: from terrane delineation to deposit-scale fluid flow. 15th Biennial SGA Meeting, Glasgow, Scotland, 27–30 August 2019, Proceedings 3:1196–1199

Hussey KJ, Huston DL, Claoué-Long JC (2005) Geology and origin of some Cu-Pb-Zn (-Au-Ag) deposits in the strangways metamorphic complex, Arunta Region: Northern Territory. Northern Territory Geol Survey Rept 17.

Huston DL, Stevens B, Southgate PN, Muhling P, Wyborn L (2006) Australian Zn-Pb-Ag ore-forming systems: a review and analysis. Econ Geol 101:1117–1157

Huston DL, Champion DC, Cassidy KF (2014) Tectonic controls on the endowment of Neoarchean cratons in volcanic-hosted massive sulfide deposits: evidence from lead and neodymium isotopes. Econ Geol 109:11–26

Huston DL, Mernagh TP, Hagemann SG, Doublier MP, Fiorentini M, Champion DC, Jaques AL, Czarnota K, Cayley R, Skirrow R, Bastrakov E (2016) Tectono-metallogenic systems—the place of mineral systems within tectonic evolution, with an emphasis on Australian examples. Ore Geol Rev 76:168–210

Huston DL, Champion DC, Czarnota K, Hutchens M, Hoggard M, Ware B, Richards F, Tessalina S, Gibson GM, Carr G (2020) Lithospheric-scale controls on zinc-lead-silver deposits of the North Australian Zinc Belt: evidence from isotopic and geophysical data. Exploring for the future: extended abstracts, Geoscience Australia, Canberra, https://doi.org/10.11636/135130

Huston DL, Doublier MP, Downes PM (2021) Geological setting, age and endowment of major Australian mineral deposits - a compilation. Geosci Austr Rec 2021/20

Huston DL, Egington B, Pehrsson S, Piercey S (2022) Global database of zinc-lead-bearing mineral deposits. Geosci Aust Rec 2022/10

Idnurm M (2000) Toward a high resolution late Palaeoproterozoic–earliest Mesoproterozoic apparent polar wander path for northern Australia. Aust J Earth Sci 47:405–430

Jackson MJ, Scott DL, Rawlings DJ (2000) Stratigraphic framework for the Leichhardt and Calvert superbasins: review and correlations of the pre-1700 Ma successions between Mt Isa and McArthur River. Aust J Earth Sci 47:381–403

Jacobsen BH (1987) Case for upward continuation as a standard separation filter for potential-field maps. Geophys 52:1138–1148

Johnson CA, Kelley KD, Leach DL (2004) Sulfur and oxygen isotopes in barite deposits of the western Brooks Range, Alaska,

and implications for the origin of the Red Dog massive sulfide deposits. Econ Geol 99:1435–1448

Johnson CA, Dumoulin JA, Buruss RA, Slack JF (2015) Depositional conditions for the Kuna Formation, Red Dog Zn-Pb-Ag-barite district, Alaska, inferred from isotopic and chemical proxies. Econ Geol 110:1143–1156

Johnson CA, Slack JF, Dumoulin JA, Kelley KD, Falck H (2018) Sulfur isotopes of host strata for Howards Pass (Yukon-Northwest Territories) Zn-Pb deposits implicate anaerobic oxidation of methane, not basin stagnation. Geology 46:619–622

Jones L, Maher J, Costelloe R, Holzschuh J, Nakamura A, Saygin E (2009) 2007 Isa-Georgetown-Charters towers seismic survey—acquisition and processing. AIG Bull 49:149–152

Kelley KD, Jennings S (2004) A special issue devoted to barite and Zn-Pb-Ag deposits in the Red Dog district, western Brooks Range, northern Alaska. Econ Geol 99:1267–1280

Kelley KD, Dumoulin JA, Jennings S (2004a) The Anarraaq Zn-Pb-Ag and barite deposit, northern Alaska: evidence for replacement of carbonate by barite and sulfides. Econ Geol 99:1577–1591

Kelley KD, Leach DL, Johnson CA, Clark JL, Fayek M, Slack JF, Ayuso RA (2004b) Textural, compositional, and sulfur isotope variations of sulfide minerals in the Red Dog Zn-Pb-Ag deposits, Alaska, USA: implications for the evolution of ore-forming fluids and depositional environment. Econ Geol 99:1509–1532

Kelley KD, Selby D, Falck H, Slack JF (2017) Re-Os systematics and age of pyrite associated with stratiform Zn-Pb mineralization in the Howards Pass district, Yukon and Northwest Territories, Canada. Mineral Deposita 52:317–335

Kirkby A, Czarnota K, Huston DL, Champion DC, Doublier MP, Bedrosian P, Duan J, Heinson G (2022) Lithospheric conductors reveal source regions of convergent margin mineral systems. Sci Rep 12:8190

Korsch RJ, Doublier MP (2016) Major crustal boundaries of Australia, and their significance in mineral systems targeting. Ore Geol Rev 76:211–228

Korsch RJ, Huston DL, Henderson RA, Blewett RS, Withnall IW, Fergusson CL, Collins WJ, Saygin E, Kositcin N, Meixner AJ, Chopping R, Henson PA, Champion DC, Hutton LJ, Wormald R, Holzschuh J, Costelloe RD (2012) Crustal architecture and geodynamics of north Queensland, Australia: insights from deep seismic reflection profiling. Tectonophys 572:76–99

Lane R, Wynne P, Poudjom Djomani Y, Stratford W, Barretto J, Ceratori Tontini F (2020) 2019 Australian national gravity grids explanatory notes. Geosci Aust Rec 2020/022

Large DE (1980) Geological parameters associated with sediment-hosted, submarine exhalative Pb-Zn deposits: an empirical model for mineral exploration. Geol Jahrb D40:59–129

Large RR, Bull SW, McGoldrick PJ, Derrick G, Carr G, Walters S (2005) Stratiform and strata-bound Zn-Pb-Ag deposits in Proterozoic sedimentary basins, northern Australia. Econ Geol 100th Anniv Vol, pp 931–963

Lawley CJM, McCafferty AE, Graham GE, Huston DL, Kelley KD, Czarnota K, Paradis S, Peter JM, Hayward N, Barlow M, Emsbo P, Coyan J, San Juan CA, Gadd MG (2022) Data-driven prospectivity modelling of sediment–hosted Zn–Pb mineral systems and their critical raw materials. Ore Geol Rev 141:104635. https://doi.org/10.1016/j.oregeorev.2021.104635

Leach DL, Bradley DC, Huston DL, Pisarevsky SA, Taylor RD, Gardoll SJ (2010) Sediment-hosted lead-zinc deposits in Earth history. Econ Geol 105:593–625

Leach DL, Sangster DF, Kelley KD, Large RR, Garven G, Allen CR, Gutzmer J, Walters S (2005) Sediment-hosted lead–zinc deposits: a global perspective. Econ Geol 100th Ann Vol, pp 561–608

Lund K (2008) Geometry of the Neoproterozoic and Paleozoic rift margin of western Laurentia: implications for mineral deposit settings. Geosphere 4:429–444

Lund K, Aleinikoff JN, Evans KV, duBray EA, Dewitt EH, Unruh DM (2010) SHRIMP U-Pb dating of recurrent Cryogenian and Late Cambrian-Early Ordovician alkalic magmatism in central Idaho: implications for Rodinian rift tectonics. Geol Soc Am Bull 122:430–453

Magnall JM, Gleeson SA, Paradis S (2020) A new subseafloor replacement model for the MacMillan Pass clastic-dominant Zn-Pb ± Ba deposits (Yukon, Canada). Econ Geol 115:953–959

Maidment DW, Huston DL, Donnellan N, Lambeck A (2013) Constraints on the timing of the Tennant Event and associated Au–Cu–Bi mineralisation in the Tennant Region, Northern Territory. Precam Res 237:51–63

McMechan ME (2012) Deep transverse basement structural control of mineral systems in the southeastern Canadian Cordillera. Can J Earth Sci 49:693–708

Miller EL, Kuznetsov N, Soboleva A, Udoratina O, Grove MJ, Gehrels G (2011) Baltica in the Cordillera? Geology 39:791–794

Monger JWH, Gibson HD (2019) Mesozoic-Cenozoic deformation in the Canadian Cordillera: the record of a "continental bulldozer"? Tectonophys 757:153–169

Moore DW, Young LE, Modene JS, Plahuta JT (1986) Geologic setting and genesis of the Red Dog zinc-lead-silver deposit, western Brooks Range, Alaska. Econ Geol 81:1696–1727

Moore TE, Wallace WK, Bird KJ, Karl SM, Mull CG, Dillon JT (1994) Geology of northern Alaska. Boulder, Colorado, The Geological Society of America, The geology of North America G-1:49–140

Morelli RM, Creaser RA, Selby D, Kelley KD, Leach DL, King AR (2004) Re–Os sulfide geochronology of the Red Dog sediment-hosted Zn-Pb-Ag deposit, Brooks Range, Alaska. Econ Geol 99:1569–1576

Morganti J (1981) Ore deposit models—4. Sedimentary-type stratiform ore deposits: some models and a new classification. Geosci Canada 8:65–75

Murphy DC, Mortensen JK, Piercey SJ, Orchard MJ, Gehrels GE (2006) Mid-Paleozoic to early Mesozoic tectonostratigraphic evolution of Yukon-Tanana and Slide Mountain terranes and affiliated overlap assemblages, Finlayson Lake massive sulphide district, southeastern Yukon. Geol Assoc Canada Spec Paper 45:75–105

Murphy FC, Hutton LJ, Walshe JL, Cleverley JS, Kendrick MA, Mclellan J, Rubenach MJ, Oliver NHS, Gessner K, Bierlein FP, Jupp B, Ailléres L, Laukamp C, Roy IG, Miller JMCL, Keys D, Nortje GS (2011) Mineral system analysis of the Mt Isa–McArthur River region, northern Australia. Aust J Earth Sci 58:849–873

Nelson J, Paradis S, Christensen J, Gabites J (2002) Canadian Cordilleran Mississippi Valley-type deposits: a case for Devonian-Mississippian back-arc hydrothermal origin. Econ Geol 97:1013–1036

Nelson JL, Colpron M, Israel S (2013) The Cordillera of British Columbia, Yukon, and Alaska: tectonics and metallogeny. Soc Econ Geol Spec Pub 17:53–109

Neumann NL, Southgate PN, Gibson GM (2009) Defining unconformities in Proterozoic sedimentary basins using detrital geochronology and basin analysis: an example from the Mount Isa Inlier, Australia. Precam Res 168:149–166

Paradis S, Nelson JL, Irwin SE (1998) Age constraints on the Devonian shale-hosted Zn-Pb-Ba deposits, Gataga district, northeastern British Columbia, Canada. Econ Geol 93:184–200

Phillips J, Duval J, Ambroziak R (1993) National geophysical data grids; gamma-ray, gravity, magnetic, and topographic data for the conterminous United States. U.S. Geol Survey Data Series 9, https://pubs.er.usgs.gov/publication/ds9, https://doi.org/10.3133/ds9

Ramos FC, Rosenberg PE (2012) Age and origin of quartz-carbonate veins associated with the Coeur d'Alene mining district, Idaho and western Montana: insights from isotopes and rare-earth elements. Econ Geol 107:1321–1339

Raymond OL, Liu S, Gallagher R, Zhang W, Highet LM (2012) Surface geology of Australia 1:1 million scale dataset 2012 editon, Geoscience Australia, Canberra, https://ecat.ga.gov.au/geonetwork/srv/api/records/c8856c41-0d5b-2b1d-e044-00144fdd4fa6

Richards FD, Hoggard MJ, White NJ, Ghelichkhan S (2020) Quantifying the relationship between short-wavelength dynamic topography and thermomechanical structure of the upper mantle using calibrated parameterization of anelasticity. J Geophys Res Solid Earth 125(9):e2019JB019062

Ridgway KD, Trop JM, Nokleberg WJ, Davidson CM, Eastham KR (2002) Mesozoic and Cenozoic tectonics of the eastern and central Alaska Range: progressive basin development and deformation in a suture zone. Geol Soc Am Bull 114:1480–1504

Ross GM (1991) Precambrian basement in the Canadian Cordillera. Can J Earth Sci 28:1133–1139

Saltus R, Brown II P, Morin R, Hill P (2008) 2006 compilation of Alaska gravity data and historical reports. US Geol Survey Data Series 264, https://pubs.usgs.gov/ds/264/

Schaeffer AJ, Lebedev S (2013) Global shear speed structure of the upper mantle and transition zone. Geophys J Int 194:417–449

Schaeffer AJ, Lebedev S (2014) Imaging the North American continent using waveform inversion of global and USArray data. Earth Planet Sci Lett 402:26–41

Scrimgeour IR, Kinny PD, Close DF, Edgoose CJ (2005) High-T granulites and polymetamorphism in the southern Arunta Region, central Australia: evidence for a 1.64 Ga accretional event. Precam Res 142:1–27

Silberling NJ, Jones DL, Monger JWH, Coney PJ (1992) Lithotectonic terrane map of the North American Cordillera. US Geol Survey Misc Invest Map I-2176, https://pubs.er.usgs.gov/publication/i2176, https://doi.org/10.3133/i2176

Skirrow RG, Cross AJ, Lecomte A, Mercadier J (2019) A shear-hosted Au-Cu-Bi metallogenic event at ~1660 Ma in the Tennant Creek goldfield (northern Australia) defined by in-situ monazite U-Pb-Th dating. Precam Res 332:105402

Slack JF, Falck H, Kelley KD, Xue GG (2017) Geochemistry of host rocks in the Howards Pass district, Yukon-Northwest Territories, Canada: sedimentary environments of Zn-Pb and phosphate mineralization. Mineral Deposita 52:565–593

Slack JF, Neymark LA, Moscati RJ, Lowers HA, Ransom PW, Hauser RL, Adams DT (2020) Origin of tin mineralization in the Sullivan Pb-Zn-Ag deposit, British Columbia: constraints from textures, geochemistry, and LA-ICP-MS U-Pb geochronology of cassiterite. Econ Geol 115:1699–1724

Southgate PN, Bradshaw BE, Domgala J, Jackson MJ, Idnurm M, Krassay AA, Page RW, Sami TT, Scott DL, Lindsay JF (2000) Chronostratigraphic basin framework for Palaeoproterozoic rocks (1730–1575 Ma) in northern Australia and implications for base-metal mineralisation. Aust J Earth Sci 47:461–483

Southgate PN, Neumann NL, Gibson GM (2013) Depositional systems in the Mt Isa Inlier from 1800 Ma to 1640 Ma: implications for Zn-Pb-Ag mineralisation. Aust J Earth Sci 60:157–173

Spinks SC, Pearce MA, Liu W, Kunzmann M, Ryan CG, Moorhead GF, Kirkham R, Blaikie T, Sheldon HA, Schaubs PM, Rickard WDA (2021) Carbonate replacement as the principal ore formation process in the Proterozoic McArthur River (HYC) sediment-hosted Zn-Pb deposit, Australia. Econ Geol 116:693–718. https://doi.org/10.5382/econgeo.479

Stacey JS, Kramers JD (1975) Approximation of terrestrial lead isotope evolution by a two-stage model. Earth Planet Sci Lett 26:207–221

Strauss JV, Macdonald FA, Taylor JF, Repetski JE, McClelland WC (2013) Laurentian origin for the North Slope of Alaska: implications for the tectonic evolution of the Arctic. Lithosphere 5:477–482

Taylor MU, McMillan NE, Dalrymple IJ, Hayward N (2017) Teena zinc-lead deposit. Austr Inst Min Metall Mon 32:483–484

Thomas WA (1977) Evolution of Appalachian-Ouachita salients and recesses from reentrants and promontories in the continental margin. Am J Sci 277:1233–1278

Thomas WA (1993) Low-angle detachment geometry of the late Precambrian-Cambrian Appalachian-Oachita rifted margin of southeastern North America. Geology 21:921–924

Thomas WA (2006) Tectonic inheritance at a continental margin. GSA Today 16:4–11

Thorpe R (2008) Release of lead isotope data in 4 databases: Canadian, western Superior, foreign, and whole rock and feldspar. Geol Survey Canada Open File 5664

Till AB (2016) A synthesis of Jurassic and Early Cretaceous crustal evolution along the southern margin of the Arctic Alaska-Chukotka microplate and implications for defining tectonic boundaries active during opening of Arctic Ocean basins. Lithosphere 8:219–237

Till AB, Dumoulin JA, Ayuso RA, Aleinikoff JN, Amato JM, Slack JF, Shanks WP III (2014) Reconstruction of an early Paleozoic continental margin based on the nature of protoliths in the Nome Complex, Seward Peninsula, Alaska. Geol Soc Am Spec Paper 506:1–28

Trop JM, Ridgway KD (2007) Mesozoic and Cenozoic tectonic growth of southern Alaska: a sedimentary basin perspective. Geol Soc Am Spec Pap 431:55–94

Valenta R (2020) Chapter 19—Walford Creek Cu-Pb-Zn-Ag-Co deposit. Northwest Mineral Province Deposit Atlas. https://smi.uq.edu.au/project/nw-mineral-province-deposit-atlas.

Wilkinson JJ (2014) Sediment-hosted zinc-lead mineralization: processes and perspectives. Geochemistry of mineral deposits: Elsevier, Amsterdam. Treatise Geochem (second Edition) 13:219–249

Williams N (1978) Studies of base metal sulfide deposits at McArthur River, Northern Territory, Australia: I. The Cooley and Ridge deposits. Econ Geol 73:1005–1035

Withnall IW, Hutton LJ (2013) Chapter 2: North Australian Craton. In Jell PA (ed) Geology of Queensland. Brisbane, Geological Survey of Queensland, pp 23–112

Wright K, James B, Pucko E (2017) Cannington Ag-Pb-Zn deposit. Aust Inst Min Metall Mon 32:507–510

Young LE (2004) A geologic framework for mineralization in the western Brooks Range, Alaska. Econ Geol 99:1281–1306

Authors and Affiliations

David L. Huston[1] [ORCID] · **David C. Champion[1]** · **Karol Czarnota[1]** · **Jingming Duan[1]** · **Matthew Hutchens[1,2]** · **Suzanne Paradis[3]** · **Mark Hoggard[4]** · **Bryant Ware[5]** · **George M. Gibson[4]** · **Michael P. Doublier[1]** · **Karen Kelley[6]** · **Anne McCafferty[6]** · **Nathan Hayward[3]** · **Fred Richards[7]** · **Svetlana Tessalina[5]** · **Graham Carr[8]**

David C. Champion
davidchampion7@gmail.com

Karol Czarnota
Karol.Czarnota@ga.gov.au

Jingming Duan
Jingming.Duan@ga.gov.au

Matthew Hutchens
matthew.hutchens@sgc.com.au

Suzanne Paradis
Suzanne.Paradis@NRCan-RNCan.gc.ca

Mark Hoggard
Mark.Hoggard@anu.edu.au

Bryant Ware
Bryant.Ware@curtin.edu.au

George M. Gibson
George.Gibson@anu.edu.au

Michael P. Doublier
Michael.Doublier@ga.gov.au

Karen Kelley
kdkelley@usgs.gov

Anne McCafferty
anne@usgs.gov

Nathan Hayward
Nathan.Hayward@NRCan-RNCan.gc.ca

Fred Richards
frichards@schmidtsciencefellows.org

Svetlana Tessalina
Svetlana.Tessalina@curtin.edu.au

Graham Carr
Graham.Carr@csiro.au

[1] Geoscience Australia, G.P.O. Box 378, Canberra, ACT 2601, Australia

[2] Southern Geoscience Consultants, 39 Richardson St, West Perth, WA 6005, Australia

[3] Geological Survey of Canada, 9860 W. Saanich Road, Sidney, BC V8L 4B2, Canada

[4] Research School of Earth Sciences, Australian National University, 142 Mills Rd, Acton, ACT 2601, Australia

[5] John de Laeter Centre, Curtin University, Building 301, Bentley, WA 6102, Australia

[6] United States Geological Survey, MS 973, Denver Federal Center, Box 25046, Denver, CO 80225-0046, USA

[7] Department of Earth and Planetary Sciences, Harvard University, 20 Oxford St, Cambridge, MA 02138, USA

[8] Division of Earth Science and Resources Engineering, Commonwealth Scientific and Industrial Research Organisation, North Ryde, NSW, Australia